



Designer flat bands: Topology and enhancement of superconductivitySi Min Chan ^{1,2}, B. Grémaud,³ and G. G. Batrouni ^{1,2,4,5}¹*Centre for Quantum Technologies, National University of Singapore, 3 Science Drive 2, 117543 Singapore*²*Department of Physics, National University of Singapore, 2 Science Drive 3, 117551 Singapore*³*Aix Marseille Université, Université de Toulon, CNRS, CPT, IPhU, AMUTech, Marseille, France*⁴*Beijing Computational Science Research Center, Beijing 100193, China*⁵*Institut de Physique de Nice, CNRS, Université Côte d'Azur, 06103 Nice, France*

(Received 4 July 2022; revised 12 September 2022; accepted 12 September 2022; published 22 September 2022)

We construct quasi-one-dimensional topological and nontopological three-band lattices with a tunable band gap and winding number of the flat band. Using full multiband mean field (MF) and exact density matrix renormalization group (DMRG) calculations, we show explicitly how the band gap affects pairing and superconductivity (SC) in a Hubbard model with attractive interactions. We obtain excellent agreement between MF and DMRG calculations. The SC weight D_s on the gapped topological, $W \neq 0$, flat band increases linearly with interaction strength U for low values and with a slope that depends on the details of the compact localized state at $U = 0$. As $U \rightarrow 0$ for the gapped nontopological flat band ($W = 0$), D_s decays with a power law faster than quadratically but slower than exponentially. In the gapless case (flat band touching the band above it), we find at low U (for both $W = 0$ and $W \neq 0$) that $D_s \propto U^\varphi$, with $\varphi < 1$. In other words, D_s increases faster than linearly for low U , thus favoring SC at weak interaction more than the gapped case. Our results reestablish that the BCS mean field and quantum metric alone are insufficient to characterize SC at weak coupling.

DOI: [10.1103/PhysRevB.106.104514](https://doi.org/10.1103/PhysRevB.106.104514)**I. INTRODUCTION**

Flat band physics has garnered wide interest since the 1990s, but this captivation has become exceptionally pronounced following the experimental realization of unconventional superconductivity in twisted bilayer graphene at a magic angle [1–4] where the appearance of a flat band is suspected to be the driving mechanism. The possibility of revealing exotic quantum phases, in particular, superconductivity on topological and nontopological flat bands, can be attributed to a unique characteristic of these dispersionless bands, where any finite interaction will be much larger than the band width, leading to strongly correlated physics at any value of the interaction.

When a particle is loaded in a flat band, the high degeneracy causes it to localize in a compact form within a few sites whose geometry depends on the details of the Hamiltonian; we will refer to this as the compact localized state (CLS). Studies on topological models have argued that, at weak coupling, isolated flat bands enhance pair formation and superconductivity (SC) and raise the BCS transition temperature T_c [5–7]. It was demonstrated, with computational and mean field methods, that a partially filled isolated flat band has superfluid weight D_s , linear in the interaction U for U much smaller than the gap, where transport is dominated by the topology of the flat band [6,8–11]. Furthermore, the slope at linearity is not simply given by the quantum metric but is accounted for, very accurately, by a proper projection on the flat band taking into account the inequivalent sublattices [9]. Recently, the quantum metric prediction for the slope was improved by introducing the notion of a minimal quantum

metric [10]. For the sawtooth lattice at a filling of $\rho = 0.5$, the quantum metric predicts the slope of D_s to be 0.6 compared to the exact density matrix renormalization group (DMRG) calculation, multiband mean field (MF) calculation, and proper projection on the flat band, all of which yield slopes of 0.40 [9]. The minimal quantum metric [10] gives a slope of 0.45, which brings it closer to the exact DMRG and MF calculations found in Ref. [9]. In two and higher dimensions, this linear behavior of D_s with U was shown to lead to a similar linear dependence of T_c on the coupling [5,7,12–14]. We recall that in dispersive bands, D_s and T_c are exponentially small as $U \rightarrow 0$, with $D_s \sim e^{-a/U}$ and $T_c \sim e^{-b/U}$.

Full multiband MF methods can accurately describe the entire range of superconducting behavior, from weak to very strong interactions where particles behave effectively like hard-core bosons on a dispersive band. Despite the changing transport mechanisms as U is increased, the full multiband MF method, which accounts for sublattice inequivalence, faithfully recovers correct results across the entire range of U [9].

When the lowest-energy flat band just touches the next dispersive band, any finite interaction will necessarily involve both bands in transport. It has been suggested, using the BCS mean field, the quantum metric, and the minimal quantum metric, that touching bands can be beneficial to superconductivity [10,15–17] resulting in $D_s \propto U \ln(\text{const}/U)$.

In this work we address two main questions. First, what is the role played in SC by topology as opposed to band flatness? In other words, suppose we have two systems with very similar-looking band structures: The lowest band is flat and separated from the next band above it, but in one system

the flat band has nonzero winding number and in the other $W = 0$. We examine how superconductivity differs in these two systems and further consider its dependence on the CLS of the flat band.

The second question is, how do the answers to the first question change when the flat band touches the band above it, i.e., in the gapless case? Both these questions are addressed in the case where the flat band filling is less than full.

Such questions have been addressed previously. However, in the case of comparing topological and nontopological flat bands, the systems that were compared had different structures. For example, in Ref. [18], the nontopological Lieb lattice was compared with the topological π -flux lattice; the former is a three-band system with the flat band in between two dispersive bands, whereas the latter is a two-band system with the flat band in the ground state. So the systems are quite different; it would be instructive to compare two very similar systems but with different topological properties.

To this end, we first focus on a quasi-one-dimensional three-band (i.e., three-orbital) system, where the winding number W , the filling on the CLS, the flat band energy, and the band gap can all be tuned by engineering the hopping parameters. We accomplish this by applying the method of Ref. [19]. We show how to obtain the Hubbard Hamiltonian for a general three-band system and the full multiband mean field required to describe these systems accurately. We outline the construction of new systems with the desired winding number, the flat band as the lowest-energy state, and the CLS on two neighboring unit cells. With the chosen W , CLS, and flat band energy, we still have the additional freedom to tune the gap through free parameters controlling the next dispersive band. We note that flat band systems have been realized experimentally with photonic lattices in two dimensions [20,21] and in quasi-one-dimension [22–24].

With these tools in hand, our main results are as follows. For the gapped topological ($W \neq 0$) system we show that, as in Ref. [9], the full multiband MF method agrees very well with exact DMRG calculations in accounting for the properties of the system over a wide range of coupling parameter and densities. In particular, we again find that for U smaller than the band gap, D_s increases linearly with U . At fixed W , band gap, and flat band energy, the relative populations of the two unit cells on which the CLS resides can be tuned and the largest slope (fastest increase) of D_s as a function of U is achieved with a symmetric population on the CLS. We also find that the slope of $D_s(U)$ depends much more sensitively on the relative populations of the two unit cells than on the quantum metric. Furthermore, unlike the Creutz and sawtooth lattices [9], we establish, in general, the dependence of the phase of the order parameters on the interaction strength U and band gap. These properties are qualitatively the same for any $W \neq 0$. For the nontopological $W = 0$, we show that a CLS on two neighboring unit cells cannot be constructed: The CLS now resides in only one cell. This then implies that transport requires the upper band. This is confirmed by DMRG and MF calculations which show that for low U , D_s is suppressed and increases slower than linearly.

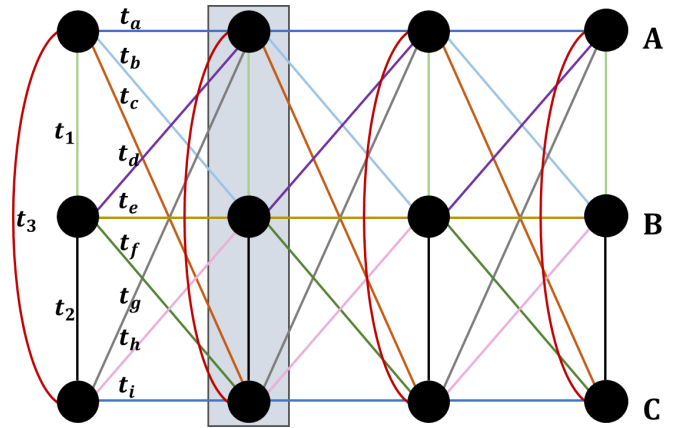


FIG. 1. Lattice with intracell hopping parameters t_1 , t_2 , and t_3 and intercell hopping parameters labeled from t_a to t_i . We consider three sublattice sites A, B, and C per unit cell (shown in the shaded rectangle) on a quasi-one-dimensional chain.

When the gap is closed and the flat band touches the band above it, the upper band will be involved in pairing and SC for any nonzero U . In this case we find that for low U and for both topological ($W = 0$) and nontopological ($W \neq 0$) bands, $D_s \propto U^\varphi$ with $\varphi < 1$. This means that, for small values of U , D_s increases faster than linearly. This power-law behavior is in disagreement with the $U \ln(\text{const}/U)$ behavior reported in the literature [10,15–17]. However, the model we consider here differs from those studied in Refs. [10,15–17] in several aspects, which could explain this difference in scaling behavior (see Sec. III B). In this paper we only consider particle densities below full filling of the flat band. So, in a three-band system, we only consider total densities below $\frac{2}{3}$.

The paper is organized as follows. In Sec. II we discuss the model Hamiltonian and how we construct it with the desired CLS and values of W , flat band energy, and gap. We also summarize our full multiband mean field method. In Sec. III we discuss the properties of the gapped and gapless topological systems $W \neq 0$, while in Sec. IV we examine the nontopological $W = 0$ case. A summary is given and our conclusions are discussed in Sec. V. Additional details and results are discussed in Appendixes A–E.

II. MODEL AND METHODS

A. Hubbard Hamiltonian: Methods

The Hubbard Hamiltonian with attractive on-site interaction on a general quasi-one-dimensional three-band system is described by

$$\begin{aligned}
 H = & \sum_{i,j,\alpha,\sigma} (t_{ij}^{\alpha,\alpha'} c_{i,\sigma}^{\alpha\dagger} c_{j,\sigma}^{\alpha'} + \text{H.c.}) - U \sum_{j,\alpha} c_{j,\downarrow}^{\alpha\dagger} c_{j,\uparrow}^{\alpha\dagger} c_{j,\uparrow}^{\alpha} c_{j,\downarrow}^{\alpha} \\
 & - \mu \sum_{j,\alpha,\sigma} c_{j,\sigma}^{\alpha\dagger} c_{j,\sigma}^{\alpha}, \quad (1)
 \end{aligned}$$

where i, j are unit cell labels, $\alpha, \alpha' = A, B, C$ are sublattice (orbital) indices, and $t_{ij}^{\alpha,\alpha'}$ is the hopping parameter between lattice sites (i, α) and (j, α') , as shown in Fig. 1. The operator $c_{j,\sigma}^{\alpha}$ ($c_{j,\sigma}^{\alpha\dagger}$) destroys (creates) a spin $\sigma = \uparrow, \downarrow$ fermion on

site i, α . The on-site Hubbard interaction parameter between a spin- \uparrow and spin- \downarrow fermions is $U > 0$; μ is the chemical potential. Choosing the hopping parameters judiciously (discussed below) yields a highly degenerate flat band. We define the filling ρ to be the average number of fermions per site, i.e., $\rho = \frac{N_{\uparrow} + N_{\downarrow}}{3L}$, where L is the number of unit cells. The superconducting behavior of these systems is probed by applying a phase gradient $c_{j,\sigma}^{\alpha} \rightarrow c_{j,\sigma}^{\alpha} e^{i\phi_j}$, where ϕ is the phase gradient Φ/L and Φ the phase twist. A defining quantity of SC, the superfluid density D_s , can then be computed from the second derivative of the thermodynamic grand potential or equivalently the ground-state energy at zero temperature [25–29],

$$D_s = \pi L \left. \frac{d^2 E_{\text{GS}}(\Phi)}{d\Phi^2} \right|_{\Phi=0}. \quad (2)$$

Superconducting transport in one-dimensional attractive Hubbard systems has also been shown to be purely pair transport [30] and, consequently, the single-particle Green's function decays exponentially while the pair Green's function decays as a power

$$G_{\sigma}^{\alpha\alpha'}(r) = \langle c_{j+r,\sigma}^{\alpha} c_{j,\sigma}^{\alpha'\dagger} \rangle \sim e^{-r/\xi}, \quad (3)$$

$$G_{\text{pair}}^{\alpha\alpha'}(r) = \langle c_{j+r,\downarrow}^{\alpha} c_{j+r,\uparrow}^{\alpha'} c_{j,\uparrow}^{\alpha'\dagger} c_{j,\downarrow}^{\alpha\dagger} \rangle \sim r^{-\omega}, \quad (4)$$

where ξ is the correlation length and ω is the power-law decay exponent.

To study the ground-state properties of this system, we use the exact DMRG computation as implemented in the ALPS library [31,32] and the full multiband MF calculation. To calculate the Green's functions with the DMRG method, we use open boundary conditions up to a system size of $L = 100$ unit cells. To calculate D_s , we need to apply a phase gradient to induce superflow which necessitates periodic boundary conditions (PBCs). To this end, we employ the method of Ref. [8], where special boundary terms are used which are effectively equivalent to PBCs. In the MF description of the Hubbard Hamiltonian, we decompose the quartic operator term $c_{j,\downarrow}^{\alpha\dagger} c_{j,\uparrow}^{\alpha\dagger} c_{j,\uparrow}^{\alpha} c_{j,\downarrow}^{\alpha}$, with the full multiband mean field expression (Appendix A) yielding the MF Hamiltonian

$$\begin{aligned} H_{\text{MF}} = & \sum_{i,j,\alpha,\sigma} (t_{ij}^{\alpha,\alpha'} c_{i,\sigma}^{\alpha\dagger} c_{j,\sigma}^{\alpha'} + \text{H.c.}) \\ & - U \sum_{j,\alpha} \rho_{\uparrow}^{\alpha} c_{j,\downarrow}^{\alpha\dagger} c_{j,\downarrow}^{\alpha} + \rho_{\downarrow}^{\alpha} c_{j,\uparrow}^{\alpha\dagger} c_{j,\uparrow}^{\alpha} \\ & - \sum_{j,\alpha} \Delta^{\alpha} c_{j,\downarrow}^{\alpha\dagger} c_{j,\uparrow}^{\alpha\dagger} + \Delta^{\alpha*} c_{j,\uparrow}^{\alpha} c_{j,\downarrow}^{\alpha} \\ & - \mu \sum_{j,\alpha,\sigma} c_{j,\sigma}^{\alpha\dagger} c_{j,\sigma}^{\alpha} \\ & + L \sum_{\alpha} U \rho_{\uparrow}^{\alpha} \rho_{\downarrow}^{\alpha} + \frac{|\Delta^{\alpha}|^2}{U}. \end{aligned} \quad (5)$$

The order parameter $\Delta^{\alpha}/U = \langle c_{j,\uparrow}^{\alpha} c_{j,\downarrow}^{\alpha} \rangle$ is complex, in general, and sublattice dependent. The average filling on sublattice α is $\rho_{\uparrow(\downarrow)}^{\alpha} = \langle c_{j,\uparrow(\downarrow)}^{\alpha\dagger} c_{j,\uparrow(\downarrow)}^{\alpha} \rangle$. Fourier transforming, we define the Nambu spinor $\Psi_k^{\dagger} = (c_{k\uparrow}^{A\dagger} \ c_{k\uparrow}^{B\dagger} \ c_{k\uparrow}^{C\dagger} \ c_{-k\downarrow}^A \ c_{-k\downarrow}^B \ c_{-k\downarrow}^C)$ and write the

Bogoliubov–de Gennes Hamiltonian

$$\begin{aligned} H_{\text{MF}}(\Phi) = & \sum_k \Psi_k^{\dagger} \mathcal{M}_k(\Phi) \Psi_k \\ & + L \sum_{\alpha} (U \rho_{\uparrow}^{\alpha} \rho_{\downarrow}^{\alpha} + \frac{|\Delta^{\alpha}|^2}{U} - U \rho_{\downarrow}^{\alpha} - \mu), \end{aligned} \quad (6)$$

where the momentum k is summed over the Brillouin zone (BZ) and $\mathcal{M}_k(\Phi)$ is a 6×6 Hermitian matrix for the three-band system (Appendix A). The phase twist Φ enters the expression through the intercell hopping terms. Diagonalizing the MF Hamiltonian (6) and solving the self-consistent equations for the order parameters and site-dependent fillings, we find the ground-state energy $E_{\text{GS}}(\Phi)$ and obtain the superfluid density D_s .

We emphasize that the full multiband MF is crucial to describe accurately the behavior of multiband systems [9]. This means that, in the most general form, (a) the order parameters are sublattice dependent and complex and (b) the sublattice-dependent filling must be taken into account as a mean-field parameter. Without these two ingredients, the agreement between MF and exact calculations deteriorates, as shown in Appendix E.

In what follows, all energies are measured in terms of our energy scale $|t_3|$, the hopping parameter between sublattices A and C on the same unit cell.

B. Flat band construction

We construct the flat band lattices using the method of Ref. [19], which we outline in Appendix B. With a choice of the CLS localized on two adjacent unit cells in a quasi-one-dimensional three-band lattice, we can obtain lattices with a flat band as the lowest-energy state. Here we represent the (not normalized) CLS wave functions on two neighboring unit cells in their most general form in real space

$$|\Psi_1\rangle = \begin{pmatrix} a \\ be^{i\beta} \\ ce^{i\gamma} \end{pmatrix}, \quad |\Psi_2\rangle = \begin{pmatrix} xe^{i\lambda} \\ ye^{i\tau} \\ ze^{i\zeta} \end{pmatrix}, \quad (7)$$

where each element is the probability amplitude on the sublattices. We can then compute the winding number W of the flat band through

$$\begin{aligned} W = & \frac{i}{\pi} \int_0^{2\pi} dk \langle \Psi_k | \partial_k \Psi_k \rangle \\ = & \frac{1}{2\pi} \int_0^{2\pi} dk \left(1 + \frac{x^2 + y^2 + z^2 - a^2 - b^2 - c^2}{2 \cos(k) + a^2 + b^2 + c^2 + x^2 + y^2 + z^2} \right) \\ = & 1 + \frac{x^2 + y^2 + z^2 - a^2 - b^2 - c^2}{\sqrt{(a^2 + b^2 + c^2 + x^2 + y^2 + z^2)^2 - 4}}, \end{aligned} \quad (8)$$

where $|\Psi_k\rangle$ is the normalized Bloch state corresponding to the CLS (Appendix B). With the condition in Eq. (8), we have the freedom to construct lattices with winding numbers of our choice (Appendix D). We write the kinetic energy part of

the Hamiltonian as H_{KE} , and H_0 and H_1 are the intracell and intercell kinetic energies, respectively (see Fig. 1),

$$H_0 = \begin{pmatrix} 0 & t_1 & t_3 \\ t_1 & 0 & t_2 \\ t_3 & t_2 & 0 \end{pmatrix}, \quad (9)$$

$$H_1 = \begin{pmatrix} t_a & t_b & t_c \\ t_d & t_e & t_f \\ t_g & t_h & t_i \end{pmatrix}, \quad (10)$$

$$H_{\text{KE}} = \begin{pmatrix} H_0 & H_1 & 0 & \cdots & 0 & H_1^\dagger \\ H_1^\dagger & H_0 & H_1 & 0 & \cdots & 0 \\ 0 & H_1^\dagger & H_0 & H_1 & \ddots & \\ \vdots & & & \ddots & & \end{pmatrix}. \quad (11)$$

Further details are outlined in Appendix B. In the examples we cover, we only consider (positive and negative) real values for the probability amplitudes in Eq. (7).

III. TOPOLOGICAL FLAT BANDS: $W \neq 0$

In this section we focus on topological flat bands with nonzero winding number $W \neq 0$. We propose two lattices, lattice \mathcal{A} and lattice \mathcal{B} , both of which have a fixed flat band energy E_{FB} but variable dispersive bands, allowing us to tune the band gap.

Here the properties of the system when there is a gap between the flat lowest-energy band and the dispersive band above it are analyzed and distinguished from the effects when

these two bands touch. In addition, we study at fixed gap and W the effect of asymmetry in the populations of the two unit cells of the CLS and the effect of changing W .

We first choose a CLS with symmetric but nonuniform populations on the two unit cells. We refer to this as lattice \mathcal{A} and its CLS is given by

$$|\Psi_1\rangle = \begin{pmatrix} \sqrt{2} \\ -\sqrt{3} \\ -\sqrt{2} \end{pmatrix}, \quad |\Psi_2\rangle = \begin{pmatrix} \sqrt{2} \\ \sqrt{3} \\ -\sqrt{2} \end{pmatrix}, \quad (12)$$

where $|\Psi_1\rangle$ and $|\Psi_2\rangle$ are the states on the two neighboring unit cells where the CLS is found. The populations on the two unit cells are the same, but within a unit cell, sublattice B has a higher population than the equal populations of sublattices A and C , shown in Fig. 2. Using Eq. (8), we show that this choice yields a winding of $W = 1$. The hopping parameters for this CLS are $t_1 = t_2 = \sqrt{7}$, $t_3 = 1$, $t_a = t_i = \frac{1}{8} + \kappa$, $t_b = t_f = \frac{1}{2}(\sqrt{7} - \sqrt{6})$, $t_c = \frac{1}{8}(13 - 2\sqrt{42}) + \kappa$, $t_d = t_h = \frac{1}{2}(\sqrt{7} + \sqrt{6})$, $t_e = 2$, and $t_g = \frac{1}{8}(13 + 2\sqrt{42}) + \kappa$ (Appendix B). The free parameter κ is used to control the band gap, as shown in Fig. 2. Fourier transforming H_{KE} , we obtain the eigenvalues λ_i which describe the band structure in Eq. (13).

The flat band energy is fixed at $E_{\text{FB}} = -4$, independent of κ . For the gapped case we set $\kappa = 0$, while for the gapless cases $\kappa = -0.375$, which has the lower two bands touching at $k = 0$ ($\frac{\partial^2 \lambda_2}{\partial k^2} |_{k=0} = \frac{4}{5}$), and $\kappa = 0.375$ is gapless at $k = \pi$ ($\frac{\partial^2 \lambda_2}{\partial k^2} |_{k=\pi} = \frac{3}{2}$), depicted in Fig. 2. Here

$$\lambda_1 = -4,$$

$$\lambda_2 = \frac{1}{8}\{16 + 18 \cos(k) + 16\kappa \cos(k) - \sqrt{6[299 + 272 \cos(k) + 27 \cos(2k)] + 2[128\kappa^2 \cos^2(k) - 128\kappa \cos(k) + 160\kappa \cos^2(k)]}\},$$

$$\lambda_3 = \frac{1}{8}\{16 + 18 \cos(k) + 16\kappa \cos(k) + \sqrt{6[299 + 272 \cos(k) + 27 \cos(2k)] + 2[128\kappa^2 \cos^2(k) - 128\kappa \cos(k) + 160\kappa \cos^2(k)]}\}. \quad (13)$$

A. Gapped case

We study first the gapped case with $E_{\text{gap}} \approx 0.7625$ ($\kappa = 0$). Figure 3 shows the superfluid density D_s versus the interaction strength U computed with the DMRG and MF methods for two fillings $\rho = \frac{1}{4}$ and $\frac{1}{3}$, where $\rho = \frac{1}{3}$ gives a half-filled flat band. The agreement is excellent between the DMRG and MF calculations for both densities and over the entire wide range of U values. In addition, the hard-core boson (HCB) approximation [33] agrees with exact and MF values of D_s at very large U , when the Cooper pairs are tightly bound. In this limit, the transport of effective hard-core bosons is governed by a dispersive model with repulsive nearest-neighbor interaction [33]. At low U , D_s rises linearly with U , as has been established for isolated flat bands. The slope of D_s against U is 0.538 for $\rho = \frac{1}{4}$ and 0.618 for $\rho = \frac{1}{3}$. In addition to D_s , the order parameters and sublattice fillings also show excellent agreement between MF and DMRG results at $\Phi = 0$, as we show in Appendix C. Furthermore, while the above features are similar to ones we have observed previously [9], this system exhibits a property not encountered before. In the

case of the Creutz flat band system we found that $\Delta^A = \Delta^B$ and both can be taken to be real; for the sawtooth system, we found that $\Delta^A \neq \Delta^B$, so in general one can be taken to be real but the other complex [9]. In addition, we found for the sawtooth lattice that when a phase gradient is applied, the phase difference between the order parameters on the two sublattices is constant and equal to the phase gradient. In the present case, we see from Eq. (12) that sublattices A and C have equal fillings and the MF calculation shows that they also have the same magnitude of the complex order parameter. However, they do not have the same phase when a phase twist is applied, $\Phi \neq 0$. By doing a global gauge transformation, the phase of $\Delta^B = |\Delta^B|e^{i\theta_B}$ can be set equal to 0. We then find that for $\Delta^A = |\Delta^A|e^{i\theta_A(U)}$ and $\Delta^C = |\Delta^C|e^{i\theta_C(U)}$, the magnitudes are equal $|\Delta^A| = |\Delta^C| \neq |\Delta^B|$ and when $\theta_B = 0$, $\theta_A = -\theta_C$. Therefore, while sublattices A and C appear to be equivalent, the phases of the order parameters are opposite in sign. This can be proved as follows. For the lattice we are considering, both matrices H_0 and H_1 [Eqs. (9) and (10), respectively] are real matrices, so one can easily prove that for each sublattice,

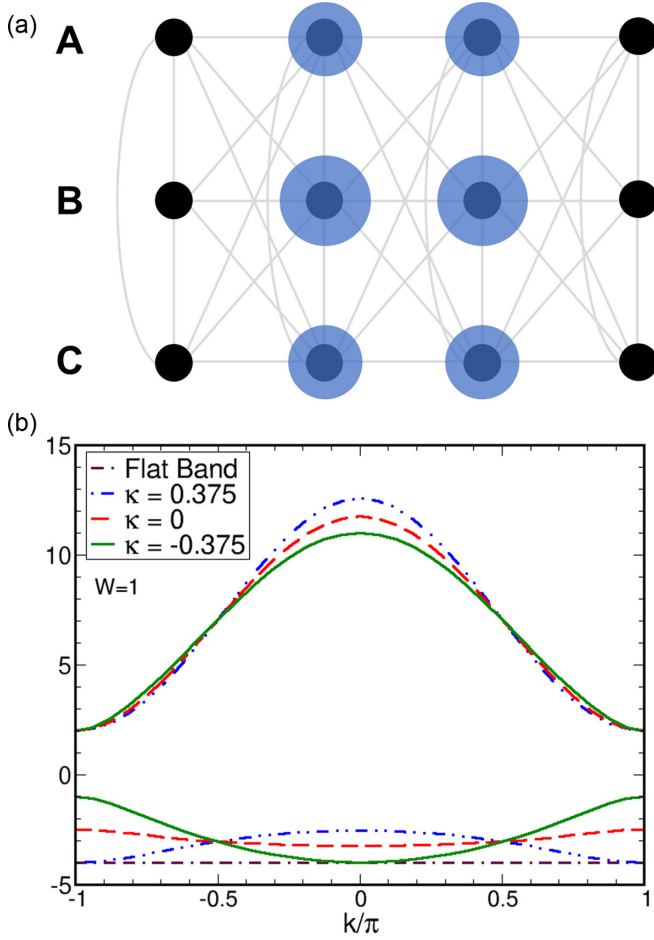


FIG. 2. (a) Compact localized states for lattice \mathcal{A} [Eq. (12)], symmetric on both unit cells. The area of the blue disks is proportional to the density on the site. (b) Band structure for $\kappa = 0.375$ (gapless at $k = \pi$), $\kappa = 0$ ($E_{\text{gap}} \approx 0.7625$), and $\kappa = -0.375$ (gapless at $k = 0$). The winding number is $W = 1$.

$\Delta^\alpha(-\phi) = \Delta^{\alpha*}(\phi)$, a situation similar to a system invariant under time reversal. In addition, the structure of H_0 and H_1 is such that exchanging sublattices A and C amounts to a paritylike symmetry, i.e., changing $i \rightarrow -i$ and $\phi \rightarrow -\phi$, in the Hamiltonian. When combined with the preceding properties, this allows us to show that $\Delta^{A*}(\phi) = \Delta^C(\phi)$ and thereby that $|\Delta^A| = |\Delta^C|$ and $\theta^A = -\theta^C$.

We also find here that, contrary to the sawtooth case, the phases of the order parameters are not constant but are U dependent. At constant U , they are proportional to the phase gradient

$$\theta_\alpha(U) = m_\alpha(U)\phi, \quad (14)$$

where $m_\alpha(U)$ is a U -dependent proportionality factor. This is shown in Fig. 4, where we see that at large U , $m_\alpha(U) \rightarrow 1$, exhibiting in that saturated limit behavior similar to that of the sawtooth lattice where the phases are not U dependent. Note that $m_\alpha(U)$ changes very rapidly for small U where D_s is linear in U . This emphasizes yet again the importance of including three distinct sublattice-dependent complex order parameters (in addition to the sublattice-dependent fillings) when describing these systems with mean field methods.

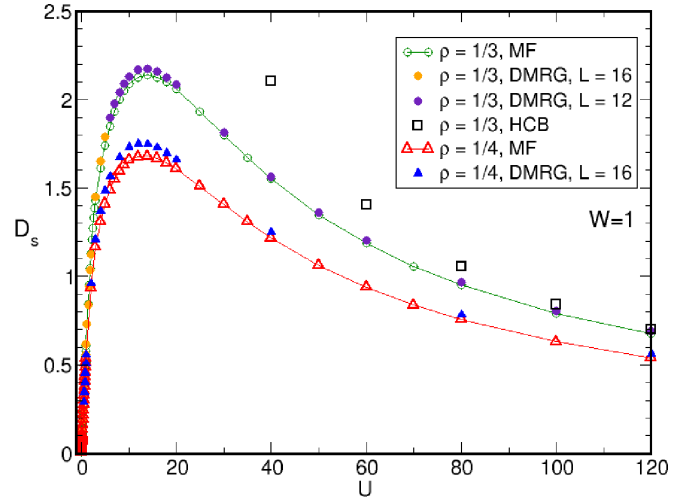


FIG. 3. Lattice \mathcal{A} ($W = 1$) gapped case ($\kappa = 0$). The superfluid density D_s is computed with DMRG and MF calculations for $\rho = \frac{1}{4}$ and $\rho = \frac{1}{3}$. The DMRG and MF calculations agree for the entire range of U for both fillings, approaching the HCB limit at strong interaction.

At this point we have examined the properties of a specific choice for the CLS, lattice \mathcal{A} [Eq. (12)]. However, as mentioned above, there is a great deal of freedom in $|\Psi_1\rangle$ and $|\Psi_2\rangle$ while keeping constant E_{FB} , W , and the gap. An interesting case to consider is a CLS with uniform site densities on all sublattices and both unit cells. We call this lattice \mathcal{B} , and its CLS is given by

$$|\Psi_1\rangle = \begin{pmatrix} 1 \\ -1 \\ 1 \end{pmatrix}, \quad |\Psi_2\rangle = \begin{pmatrix} 1 \\ 1 \\ 1 \end{pmatrix}. \quad (15)$$

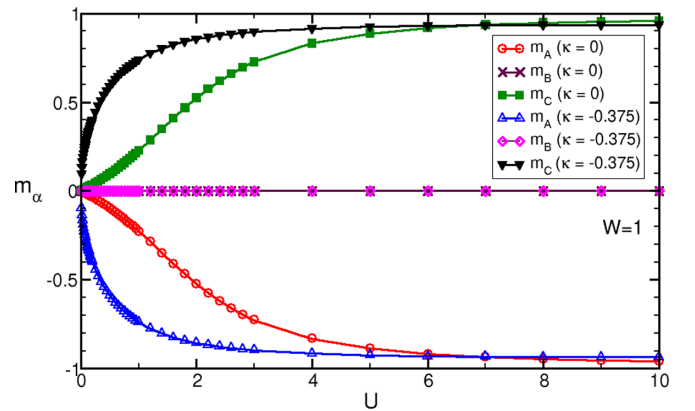


FIG. 4. Lattice \mathcal{A} ($W = 1$). The proportionality factor $m_\alpha(U)$ [Eq. (14)] is plotted versus U for the gapped and gapless band structures of lattice \mathcal{A} . At large U , $m_\alpha \rightarrow 1$ and the U dependence saturates. The filling is $\rho = \frac{1}{3}$. The same behavior is observed at other fillings.

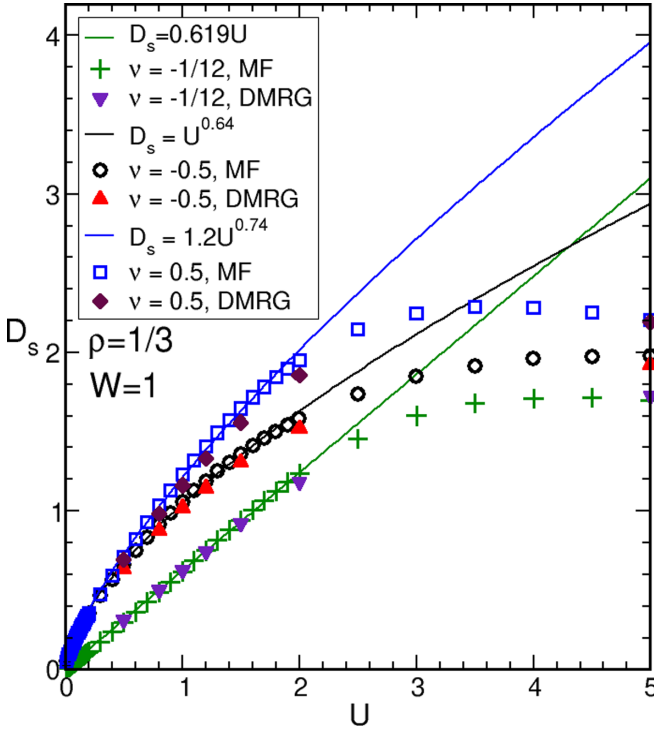


FIG. 5. Lattice \mathcal{B} ($W = 1$). The SC weight D_s is plotted vs U with $\nu = -\frac{1}{12}$ ($E_{\text{gap}} = 1$), $\nu = -0.5$ (gapless at $k = 0$), and $\nu = 0.5$ (gapless at $k = \pi$). We observe a linear relation for the gapped case and $D_s \sim U^\varphi$, with $\varphi < 1$, for the touching bands. The filling is $\rho = \frac{1}{3}$.

This choice has $W = 1$ and intracell and intercell hopping Hamiltonians

$$H_0 = \begin{pmatrix} 0 & -1 & -1 \\ -1 & 0 & 1 \\ -1 & 1 & 0 \end{pmatrix}, \quad H_1 = \begin{pmatrix} \nu & -1 & -1 - \nu \\ 0 & 1 & 1 \\ -\nu & 0 & \nu \end{pmatrix}, \quad (16)$$

where ν is a parameter used to tune the gap. The eigenvalues describing the three bands are

$$\begin{aligned} \lambda_1 &= -2, \\ \lambda_2 &= 1 + \cos(k) + 2\nu \cos(k) \\ &\quad - \sqrt{4\nu^2 \cos^2(k) + \cos^2(k) + 4 \cos(k) + 3}, \\ \lambda_3 &= 1 + \cos(k) + 2\nu \cos(k) \\ &\quad + \sqrt{4\nu^2 \cos^2(k) + \cos^2(k) + 4 \cos(k) + 3}. \end{aligned} \quad (17)$$

These bands touch at $k = 0$ for $\nu = -0.5$ ($\frac{\partial^2 \lambda_2}{\partial k^2} \big|_{k=0} = \frac{4}{3}$) and at $k = \pi$ for $\nu = 0.5$ ($\frac{\partial^2 \lambda_2}{\partial k^2} \big|_{k=\pi} = 2$) with a flat band energy $E_{\text{FB}} = -2$, independent of ν . For the gapped case, we choose $\nu = -\frac{1}{12}$ for a band gap of $E_{\text{gap}} = 1$.

Figure 5 shows that, in the gapped case ($\nu = -\frac{1}{12}$), D_s is again linear in U for lattice \mathcal{B} and small U with a slope of 0.619. Naively, one might expect the uniformity of site fillings to persist when $U \neq 0$. On the contrary, we find that for any finite U , the uniform density of the CLS of lattice \mathcal{B}

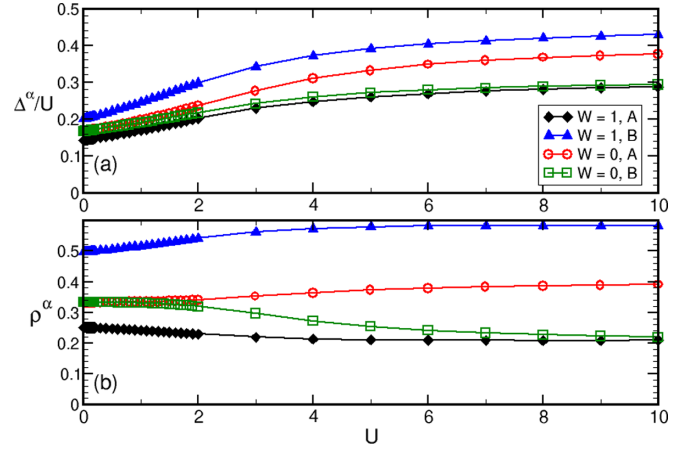


FIG. 6. The (a) MF order parameters and (b) fillings on sublattices A and B for isolated topological (lattice \mathcal{B} , $W = 1$) and nontopological (lattice \mathcal{C} , $W = 0$) flat bands with $E_{\text{gap}} = 1$ and equal filling on all sites of the CLS. Lattice \mathcal{B} with $W = 1$ has $\Delta^A \neq \Delta^B$ and $\rho^A \neq \rho^B$ for any finite U . For lattice \mathcal{C} ($W = 0$), the sublattice-dependent order parameters and fillings go smoothly to equal values as $U \rightarrow 0$. In both cases, $|\Delta^A| = |\Delta^C|$ and $\rho^A = \rho^C$, but the order parameters on all three sublattices have different phases at $\phi \neq 0$. When $W = 0$, Δ^B (ρ^B) is smaller than $\Delta^A = \Delta^C$ ($\rho^A = \rho^C$), in contrast to the topological $W = 1$ cases. The filling is $\rho = \frac{1}{3}$.

[Eq. (15)] is broken and the sublattices again become distinct. This is seen clearly in Fig. 6, where (for $W = 1$, the case we examine here) $\Delta^A/U \neq \Delta^B/U$ and $\rho^A \neq \rho^B$ for all $U > 0$. The phases of the order parameters, Δ^A and Δ^C , behave in the same way as for lattice \mathcal{A} , i.e., they are equal and opposite in sign when the global gauge is fixed so that Δ^B is real. For lattices \mathcal{A} and \mathcal{B} with a symmetric CLS on both unit cells, we obtain approximately equal slopes of D_s against U for the gapped case (Figs. 5 and 7) despite the differences in band gap, hopping potentials, and flat band energy. One might argue that this should be obvious, as transport is dominated by the flat band and they have equal winding numbers. However, with the freedom of constructing asymmetric CLSs with the same W , E_{gap} , and E_{FB} as the symmetric ones, we demonstrate the dominant effect of the CLS symmetry on SC properties. In Appendix D we show in detail that a symmetric CLS on the flat band is the most favorable in terms of optimizing the SC, for $W = 1$. Maintaining a winding of 1, $E_{\text{FB}} = -4$, and $E_{\text{gap}} \approx 0.7625$, we find that the more symmetric the CLS is, the faster D_s increases with U . We attribute this to the overlap of Wannier functions which increases with the symmetry of the CLS site densities, thus optimizing D_s . Very interestingly, as the slope of the linear part of $D_s(U)$ (which we denote by S) decreases due to the asymmetry, the value of the integral over the BZ of the quantum metric remains rather constant: S is much more sensitive to the CLS than to the quantum metric (Appendix D). Additionally, the site fillings, order parameters, and band structures do not vary much across the cases considered, despite the significant difference in D_s .

As mentioned above, the winding number of the flat band can be tuned. To illustrate this, we constructed Hamiltonians with $W = \frac{1}{2}$, for several CLS configurations, and performed a study similar to that for $W = 1$ (lattices $\mathcal{D}1$, $\mathcal{D}2$, and $\mathcal{D}3$

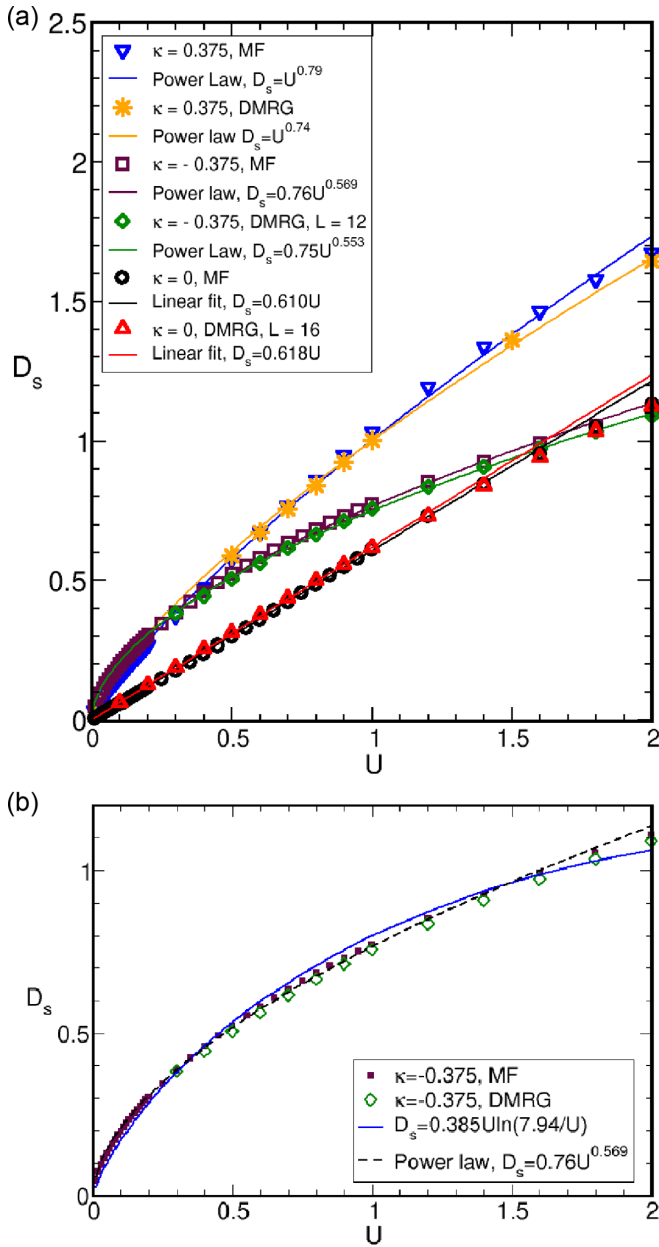


FIG. 7. (a) Low- U behavior of D_s for lattice \mathcal{A} for $\rho = \frac{1}{3}$, with $\kappa = -0.375$ (touching at $k = 0$), $\kappa = 0$ (gapped), and $\kappa = 0.375$ (touching at $k = \pi$) showing that touching bands can drastically improve superconductivity at weak attraction. There is a clear power-law dependence, with power exponent less than 1 for both $\kappa = -0.375$ and 0.375 . (b) Comparison of the power law $D_s \propto U^\varphi$ and $D_s \propto U \ln(\text{const}/U)$ fits. The data are inconsistent with a $U \ln(\text{const}/U)$ behavior.

in Appendix D). When $W = \frac{1}{2}$, Eq. (8) dictates that the CLS must be asymmetric. Qualitatively, the behavior of D_s is similar to the $W = 1$ case in that it exhibits a linear part at low U . In addition, Δ^A , Δ^B , Δ^C , and their phases are unequal for all sublattices and dependent on U . As we reduce the filling on one unit cell of the CLS, increasing the asymmetry, we find the slope \mathcal{S} of $D_s(U)$ decreases. In other words, for the same sublattice, the occupation must be comparable on both unit cells of the CLS to increase D_s .

We thus conclude this section by stating that to optimize D_s on the isolated topological flat band, one should identify the case with the most symmetric CLS. Specifically, when $W = 1$, the occupation on the optimized CLS will be truly symmetric.

B. Gapless cases

It has been argued that nonisolated flat bands may be beneficial to SC [10,15–17] with D_s increasing as $U \ln(\text{const}/U)$ for small U , i.e., faster than linear. Here we study this situation where a dispersive band touches the flat band below it and what effect it has on SC. To this end, we consider both our lattices \mathcal{A} and \mathcal{B} with $W = 1$. The former has a symmetric CLS but with site densities which are not uniform [Eqs. (12) and (13)]; the latter has a CLS with uniform site densities [Eqs. (15)–(17)]. For lattice \mathcal{A} we take $\kappa = -0.375$ (bands touching at $k = 0$) and $\kappa = 0.375$ (bands touching at $k = \pi$); for lattice \mathcal{B} , we take $\nu = -\frac{1}{2}$ (bands touching at $k = 0$) and $\nu = \frac{1}{2}$ (bands touching at $k = \pi$).

In Figs. 5 and 7 we exhibit the behavior of D_s at low values of U for both these gapless systems and we also include the corresponding linear gapped case for comparison. We see that for all gapless cases (bands touching at $k = 0, \pi$), a power law fit $D_s \propto U^\varphi$ with $\varphi < 1$ describes the dependence very well for both the DMRG and MF calculations. This means that for small U , D_s increases faster with U when the bands touch than when there is a gap where the behavior is linear; this favors SC because the carrier density is higher at low U . However, in both gapped and gapless cases, the Δ increase linearly with U . In the quasi-one-dimensional case we examine here, there is no finite-temperature transition between SC and a normal phase: True SC is present at $T = 0$ only. If the $D_s \propto U^\varphi$ with $\varphi < 1$ and $\Delta^\alpha \propto U$ behavior persists in higher dimensions, that would mean that T_c may not be enhanced when the bands touch, since $\Delta^\alpha \propto U$, even though the carrier density itself is enhanced. In Fig. 7(b) we compare the quality of fits of the power law and the $U \ln(\text{const}/U)$. We find the power law to be in much better agreement with the MF and DMRG calculations and over a wider range of U ; we therefore argue that the power law is more appropriate than the logarithmic form to describe D_s . We point out two main differences between our systems and those discussed in Refs. [10,15–17] where the logarithmic behavior is observed: (a) Our systems are quasi-one-dimensional whereas those in Refs. [10,15–17] are two dimensional and (b) in our systems, unlike the two-dimensional ones, when the gap between the flat band and the second band shrinks, the CLS remains unchanged and consequently the quantum metric and its BZ integral remain constant. In the two-dimensional systems mentioned, the logarithmic behavior of D_s has been attributed to a logarithmic divergence of the BZ integral of the diagonal quantum metric [10,15–17]. In our case, as we mentioned, the CLS remains unchanged as the gap shrinks and the bands touch and consequently no such divergence occurs.

We note that the power-law exponents are larger when the curvature of the dispersive band is larger which, for these two lattices, happens at $k = \pi$. In Fig. 8 we show D_s over a very wide range of U for two densities when the bands touch at $k = 0$. We see again that agreement between our multiband MF and exact DMRG calculations is excellent over the entire

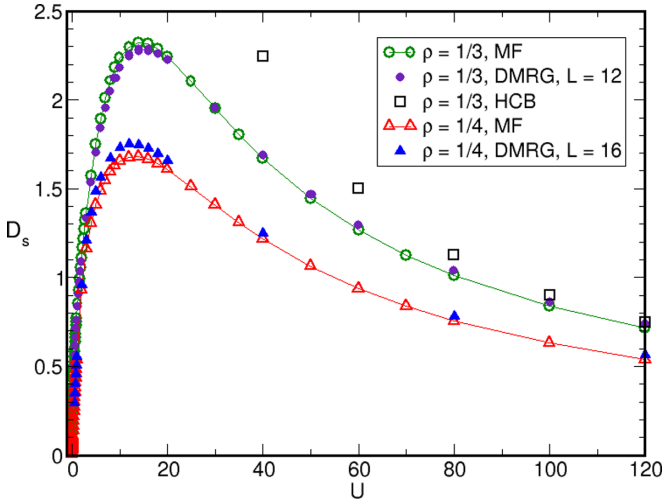


FIG. 8. Lattice \mathcal{A} ($W = 1$), gapless at $k = 0$ ($\kappa = -0.375$). The superfluid density is obtained with the MF and exact DMRG calculations for two fillings $\rho = \frac{1}{4}$ and $\frac{1}{3}$. Even with touching bands, our MF calculation agrees very well with the DMRG calculation.

range of U , as it was in the gapped case. The order parameters are shown in Appendix C. In addition, we use this case to illustrate the inaccuracy of the MF calculation when the site densities are not included as variational MF parameters (Appendix E).

As a result of pairing, the single-particle Green's functions exhibit exponential decay, while the pair Green's functions decay with a power law since the system is SC [30] [Eq. (3)]. The correlation length ξ extracted from the decay exponent of the single-particle Green's function obtained with our MF method agrees very well with that obtained with the DMRG method, which we show for lattice \mathcal{B} in Fig. 9(a). Recalling that the correlation length typically diverges exponentially for dispersive bands [30] as $U \rightarrow 0$, we find here a different behavior for the correlation length on the gapped and gapless flat bands. As previously established in Ref. [9] for the Creutz and sawtooth lattices, the correlation length goes to a constant, less than one lattice spacing for the isolated flat band as $U \rightarrow 0$. We observe here this same behavior in the gapped case. However, in the gapless case, the single-particle correlation length ξ diverges as a power law $\xi \sim U^{-P}$, as $U \rightarrow 0$, i.e., much slower than in the dispersive case. The power-law decay of the pair Green's function is characterized by the exponent ω , which we calculate with the DMRG method. We find that ω increases with U and is larger in the gapped case than in the gapless case. The lower values of ω in the gapless case are consistent with the larger values of D_s than for the isolated flat band in the same range of U (Fig. 5). In other words, the smaller the ω , the slower the decay of the quasi-long-range order and the larger the D_s . We point out that the pair Green's functions cannot be obtained using the MF method.

IV. NONTOPOLOGICAL FLAT BANDS: $W = 0$

In this section we study pairing and superconductivity in a system with a nontopological flat band with zero winding number $W = 0$. To this end, we exploit the tunability of the

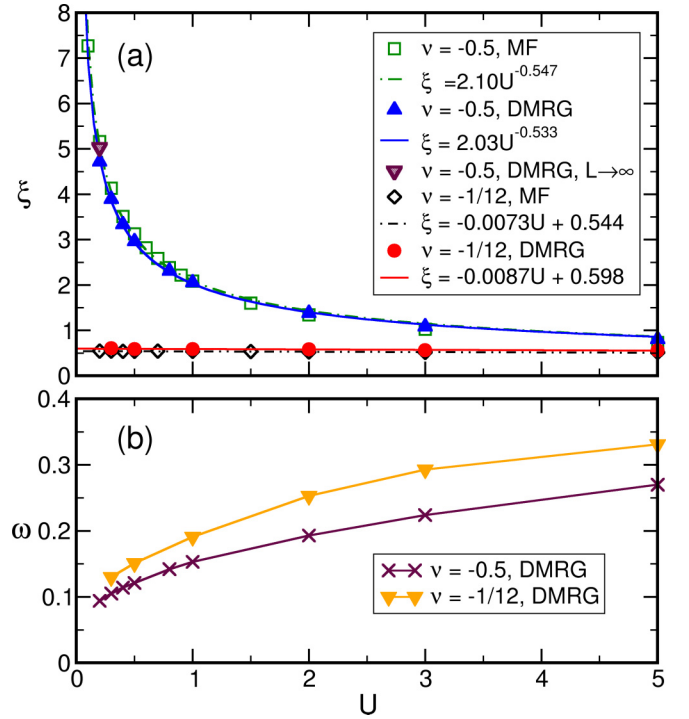


FIG. 9. Lattice \mathcal{B} . (a) Correlation length ξ with fitted functions for both MF and DMRG calculations ($L = 100$). For $U = 0.2$, we include the extrapolated value $\xi(L \rightarrow \infty)$ for touching bands, where finite-size effects result in a slightly increased discrepancy between the MF and DMRG results at low U . (b) Pair Green's-function power-law decay exponent ω obtained from the DMRG calculation, as a function of U for the cases where $E_{\text{gap}} = 1$ and $\nu = -\frac{1}{12}$ and the bands are gapless at $k = 0$ and $\nu = -0.5$. The filling is $\rho = \frac{1}{3}$.

winding number in the approach we explained above and tune the CLS to yield a Hamiltonian with $W = 0$ for the flat band. We find that to accomplish this, the CLS must be localized within only one unit cell rather than two neighboring unit cells as is the case for the topological bands (details in Appendix B). We call this nontopological case lattice \mathcal{C} . We choose it to have equal sublattice densities on all sites and a flat band energy $E_{\text{FB}} = -2$. The CLS is given by

$$|\Psi_1\rangle = \begin{pmatrix} 1 \\ 1 \\ 1 \end{pmatrix} \quad (18)$$

and the hopping terms are

$$H_0 = \begin{pmatrix} 0 & -1 & -1 \\ -1 & 0 & -1 \\ -1 & -1 & 0 \end{pmatrix}, \quad H_1 = QKQ, \quad Q = \frac{1}{3} \begin{pmatrix} 2 & -1 & -1 \\ -1 & 2 & -1 \\ -1 & -1 & 2 \end{pmatrix}. \quad (19)$$

In this case K is an arbitrary nonzero 3×3 matrix. To have a band gap of 1, a possible, but not unique, choice for K is

$$K = \begin{pmatrix} 0 & 0 & 0 \\ 0 & 0 & 0 \\ 2 & 0 & 0 \end{pmatrix}, \quad (20)$$

which gives the eigenvalues

$$\begin{aligned} \lambda_1 &= -2, \\ \lambda_2 &= \frac{1}{3}[3 - 2 \cos(k) - \sqrt{14 + 2 \cos(k)}], \\ \lambda_3 &= \frac{1}{3}[3 - 2 \cos(k) + \sqrt{14 + 2 \cos(k)}]. \end{aligned} \quad (21)$$

For the gapless case, we use the construction

$$K = \begin{pmatrix} 0 & 0 & \frac{3}{2} + \varrho \\ 0 & 0 & 0 \\ \frac{3}{2} - \varrho & 0 & 0 \end{pmatrix} \quad (22)$$

for the bands touching at $k = 0$ and

$$K = \begin{pmatrix} 0 & 0 & -\frac{3}{2} + \varrho \\ 0 & 0 & 0 \\ -\frac{3}{2} - \varrho & 0 & 0 \end{pmatrix} \quad (23)$$

for the bands touching at $k = \pi$, where ϱ is a parameter which controls the upper bands and consequently their curvature. We then arrive at

$$\begin{aligned} \lambda_1 &= -2, \\ \lambda_2 &= 1 \mp \cos(k) - \frac{\sqrt{6}}{3} \sqrt{(3 - \varrho^2) \cos(2k) + 3 + \varrho^2}, \\ \lambda_3 &= 1 \mp \cos(k) + \frac{\sqrt{6}}{3} \sqrt{(3 - \varrho^2) \cos(2k) + 3 + \varrho^2} \end{aligned} \quad (24)$$

for the gapless case and $-$ ($+$) for band touching at $k = 0$ ($k = \pi$) in λ_2 and λ_3 , and we can calculate exactly the curvature of the second band.

Before examining the properties arising from filling lattice \mathcal{C} , we point out some apparent differences between the band structures of the $W \neq 0$ and $W = 0$ cases. For the $W \neq 0$ lattices, we have the option of having the bands touch at $k = 0$ or at $k = \pi$, but do not have the freedom to tune the curvature at the point where they touch. Here we can control both the touching point and the curvature. For a fixed ϱ , the band curvature is equal where they touch, at $k = 0$ and $k = \pi$.

First, we highlight the differences between lattices \mathcal{B} ($W = 1$ with uniform site densities in the CLS) and \mathcal{C} ($W = 0$ with uniform site densities in the CLS) in terms of sublattice equivalence. For comparison, we use the isolated bands case. Figure 6 shows that for any nonzero U , no matter how small, the order parameters and site densities are no longer uniform in the $W = 1$ case, despite supporting a uniform CLS. On the other hand, for $W = 0$, we see that as $U \rightarrow 0$, the order parameters on the two sublattices approach each other and merge at low U . The same behavior is observed for the site densities. Furthermore, while the magnitudes of the pairing order parameters on sublattices A and C are equal, their phases for $\Phi \neq 0$ are not. We thus reiterate that even when the CLS is uniform, it is prudent always to consider independent complex order parameters and site densities as variational parameters when applying the MF method.

Even though the pairing parameters $\Delta^{A,B}/U$ are finite as $U \rightarrow 0$ in the isolated flat band case (Fig. 6), indicating robust pairing for any U , the superfluid density itself is suppressed: It decays as a power as $U \rightarrow 0$. For $E_{\text{gap}} = 1$, the MF calculation yields $D_s = 0.028U^{2.32}$. This power-law decay of D_s can be understood through projecting the MF onto the flat band and examining the terms that contribute [9]. The leading term proportional to U vanishes for $W = 0$ under this construction, which has a CLS localized on one unit cell. As a result, the first nonzero term is of a higher order. The DMRG convergence becomes increasingly difficult and time consuming at low values of U . The flat nontopological band cannot contribute to transport through either the band curvature or topology, resulting in an increased number of DMRG sweeps and states required at low U where band mixing is highly suppressed.

When the flat band touches the band above it, we find that D_s is strongly enhanced and grows as a power $D_s \propto U^\varphi$ with the exponent $\varphi < 1$ (Fig. 10). Interestingly, this is exactly the same behavior we find when the topological flat band touches the band above it. In addition, as mentioned above, in this case we also have the freedom to tune the curvature of the second band. In our construction, the limits of the curvature are (while avoiding band crossing) at $\varrho = 3/\sqrt{2}$ ($\frac{\partial^2 \lambda_2}{\partial k^2}|_{k=0} = 0$) and $\varrho = 0$ ($\frac{\partial^2 \lambda_2}{\partial k^2}|_{k=0} = 3$). We show in Fig. 10 three examples of curvatures (the aforementioned and $\varrho = 1.5$ and $\frac{\partial^2 \lambda_2}{\partial k^2}|_{k=0} = 1.5$) and their corresponding D_s . Transport is dominated by the upper band in the nontopological case and the effective mass of fermions on the upper band decreases with increasing band curvature. However, with the bands touching and degenerate states supported by the flat band, the behavior of D_s as $U \rightarrow 0$ is unlike the exponential decay of a dispersive band. Consequently, increasing the curvature of the second band decreases the power exponent φ , with $D_s \propto U^\varphi$, where the steepest curvature of the second band is most beneficial towards optimizing the superfluid behavior.

In all cases, the phases of the order parameters behave similarly to Fig. 4, in that they differ for all three sublattices and are dependent on the interaction strength. We notice that the isolated band case has significantly smaller SC density D_s than the gapless case for the entire range of U , unlike the $W \neq 0$ case where the SC densities are comparable once there is band mixing, i.e., once U is of the order of the gap energy.

When the bands touch at $k = \pi$, we observe identical behavior, where for the same ϱ and upper band curvature, the values of D_s , order parameters, and sublattice fillings are equal to when the bands touch at $k = 0$. This highlights the fact that the superfluid weight on the gapless nontopological flat band is only controlled by the upper band curvature. Additionally, the correlation length on nontopological flat bands as $U \rightarrow 0$ is identical to that in Fig. 9, with power-law divergence for touching bands and a constant, less than one lattice spacing for isolated flat bands.

We remark that while for $W = 0$ the qualitative agreement between the MF and DMRG calculations is excellent, the quantitative agreement for $W \neq 0$ is much better. We believe this is due to the fact that the CLS for $W = 0$ is on a single unit cell with the consequence that hopping between unit cells, i.e., transport, requires the participation of the higher band which

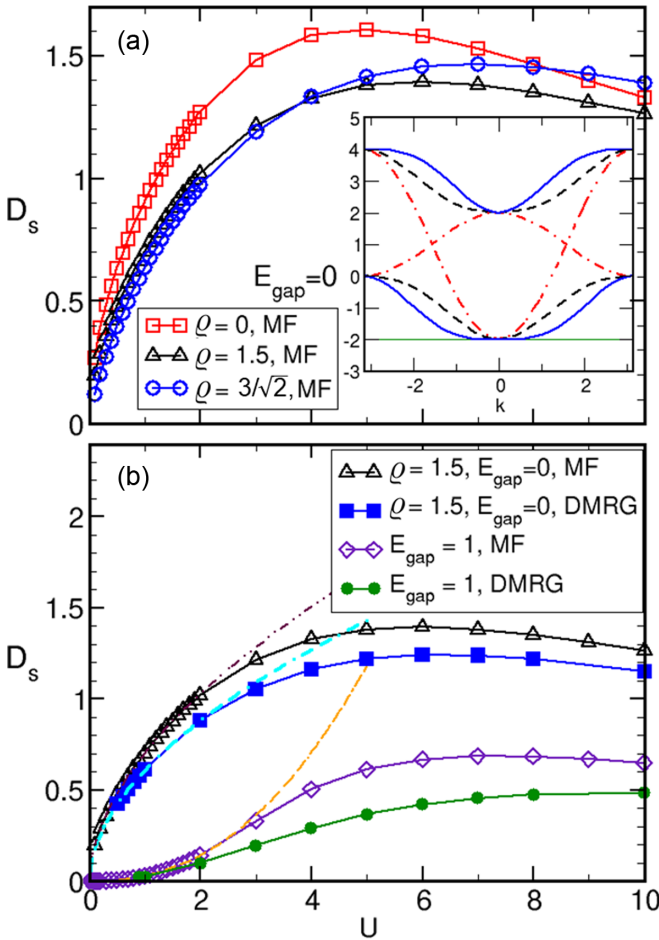


FIG. 10. Plot of D_s vs U for $W = 0$ isolated and nonisolated flat bands. (a) The MF calculation shows that when the bands touch, the curvature and optimization of $D_s(U)$ depend on the curvature of the second band, controlled by ϱ . The inset shows the band structure of lattice \mathcal{C} for $\varrho = 0, 1.5, 3/\sqrt{2}$ in the gapless case. Increasing ϱ decreases the curvature of the second band. (b) Suppressed superconductivity in the gapped case behaves as a power law, with the fit $D_s = 0.028U^{2.32}$ at low U for the MF calculation. While the DMRG and MF calculations differ numerically, the power dependences of D_s obtained from both methods agree (shown for $\varrho = 1.5$). For the DMRG calculation $D_s = 0.612U^{0.53}$ and for the MF calculation $D_s = 0.7U^{0.55}$. The filling is $\rho = \frac{1}{3}$.

is a higher-order process. On the other hand, for $W \neq 0$, the CLS is spread over two unit cells to begin with, which makes transport easier.

V. CONCLUSION

In this work we have extended the method of Ref. [19] and shown how to generate flat band Hamiltonians with tunable winding number for the flat band, as well as a tunable gap and CLS configuration. We then used our construction to study, in three-band systems, the effects on pairing and superconductivity of the winding number, the CLS configuration, and the gap between the flat band and the first band above it, for both topological and nontopological flat bands. To this end we used both full multiband MF and exact DMRG calculations

TABLE I. Dependence of the superfluid density D_s on U (for small U) for the cases we study in this work.

Band topology	Band gap	Behavior of D_s
$W \neq 0$	isolated	$D_s \propto U$
$W \neq 0$	gapless	$D_s \propto U^\varphi, \varphi < 1$
$W = 0$	isolated	$D_s \propto U^\chi, \chi > 2$
$W = 0$	gapless	$D_s \propto U^\varphi, \varphi < 1$

and found excellent agreement between them especially in the topological cases. Our results led us to emphasize again that, in order to get accurate MF results, it is crucial to consider both the order parameters and the site densities as separate variational MF parameters on all sublattices.

Specifically, we found for the gapped topological case $W \neq 0$ that, for low- U values, D_s grows linearly with a slope which depends sensitively on the choice of the CLS fillings even when W and the integral over the BZ of the quantum metric remain fixed. The optimal CLS choice (the one which gives the largest slope) has symmetric site densities on the two unit cells because this maximizes the overlap of the Wannier functions of a distinct CLS. Interestingly, if the CLS is chosen with uniform site densities on all sites, the uniformity breaks down for any $U \neq 0$: Sublattices A and C continue to have the same density but not sublattice B . In the case of a gapped nontopological flat band, we find that D_s is suppressed for U smaller than the gap; it grows slowly as a power larger than 2 until U is of the order of the band gap at which point band mixing helps superconductivity.

In the gapless case, when the bands touch, we showed clear evidence of a power-law dependence $D_s \sim U^\varphi$ ($\varphi < 1$), not the logarithmic form $D_s \sim U \ln(\text{const}/U)$, for both topological and nontopological flat bands. Superconductivity at low U is therefore enhanced when the topological or nontopological flat band touches the band above it.

The dependence of D_s on U for small values of U is summarized in Table I. In all cases we studied, the order parameter Δ^α/U acquires large values for any finite U , as long as $\rho^\alpha \neq 0$. The phase difference of the order parameters was found to depend on Φ , U , and the band structure, unlike previous two-band cases studied [9]. Furthermore, we showed that, as $U \rightarrow 0$, the single-particle correlation length (extracted from the single-particle Green's function), which is a measure of the pair size, diverges as a power when the bands touch, but tends to a constant less than one lattice spacing in the gapped case. The pairs remain very small when the system is gapped and their size diverges in the gapless case, but the divergence is slower than in the dispersive band case where it is exponential.

Since in our three-band model the order parameter Δ^α is not uniform (i.e., it is sublattice dependent), we find that

$$[\mathcal{K}, \mathcal{D}] \neq 0. \quad (25)$$

According to Ref. [34], this interband hybridization induced by the singlet pairing has a clear signature in the frequency dependence of the off-diagonal Green's function $F(\omega)$, the Fourier transform of the time correlator $\langle c_{i\downarrow}^\alpha(t)c_{i\uparrow}^{\alpha'}(0) \rangle$. For standard single-band BCS superconductors, both S -wave

singlet and P -wave triplet pairing exhibit an even behavior of $F(\omega)$ as a function of the frequency ω . On the other hand, in the present multiband models and for different band indices $\alpha \neq \alpha'$, the sublattice pairing imbalance leads to an odd behavior of $F(\omega)$, i.e., it exhibits S -wave singlet pairing with an odd symmetry when exchanging sublattices. See Ref. [34] for more details.

Our results here offer insight into enhancement of superconductivity in quasi-one dimensional systems and a methodology to finding optimized Hamiltonians. With the increasing experimental ability to realize designer systems governed by model Hamiltonians exhibiting a flat band [20–24], our results can provide a practical road map.

The Hamiltonians we studied here do not have a chiral symmetry. It is possible to construct such models [19], but due to the chiral symmetry, the band structure must be symmetric about zero energy. This means that if we want a flat band in the ground state, the system must have an even number of orbitals. An example of the two-band system (the Creutz lattice) was studied in Ref. [9]. The next step would be to study the four-band model (four coupled chains). Our multiband MF method can be easily applied in this situation, but exact DMRG calculations will be rather challenging due to the large number of sites.

ACKNOWLEDGMENTS

S.M.C. was supported by a National University of Singapore President's Graduate Fellowship. The DMRG computations were performed with the resources of the National Supercomputing Centre, Singapore. This research was supported by the National Research Foundation, Prime Minister's Office and the Ministry of Education (Singapore) under the Research Centres of Excellence program. This project has also received funding from Excellence Initiative of Aix-Marseille University, A*MIDEX, a French Investissements d'Avenir program through the IPhU (Grant No. AMX-19-IET-008) and AMUtech (Grant No. AMX-19-IET-01X) institutes.

APPENDIX A: MULTIBAND MEAN FIELD HAMILTONIAN

The full multiband mean field is derived by decomposing the quartic interaction term in the Hamiltonian with mean field parameters Δ^α and ρ_σ^α for each sublattice. As in Ref. [9], but with three independent sublattices, we write a trial Hamiltonian

$$\begin{aligned}
 H_{\text{trial}} &= H_K \\
 &- U \sum_{j,\alpha} \rho_\uparrow^\alpha c_{j,\downarrow}^{\alpha\dagger} c_{j,\downarrow}^\alpha + \rho_\downarrow^\alpha c_{j,\uparrow}^{\alpha\dagger} c_{j,\uparrow}^\alpha \\
 &- \sum_{j,\alpha} \Delta^\alpha c_{j,\downarrow}^{\alpha\dagger} c_{j,\uparrow}^{\alpha\dagger} + \Delta^{\alpha*} c_{j,\uparrow}^\alpha c_{j,\downarrow}^\alpha, \\
 H_K &= \sum_{i,j,\alpha,\sigma} (t_{ij}^{\alpha,\alpha'} c_{i,\sigma}^{\alpha\dagger} c_{j,\sigma}^{\alpha'} + \text{H.c.}) \\
 &- \mu \sum_{j,\alpha,\sigma} c_{j,\sigma}^{\alpha\dagger} c_{j,\sigma}^\alpha, \tag{A1}
 \end{aligned}$$

with mean field parameters Δ^α and ρ_σ^α . The Gibbs-Bogoliubov inequality [35] gives

$$\begin{aligned}
 F &\leq F_{\text{trial}} - \left\langle U \sum_{j,\alpha} c_{j,\downarrow}^{\alpha\dagger} c_{j,\uparrow}^{\alpha\dagger} c_{j,\uparrow}^\alpha c_{j,\downarrow}^\alpha \right\rangle_{\text{trial}} \\
 &+ \left\langle U \sum_{j,\alpha} \rho_\uparrow^\alpha c_{j,\downarrow}^{\alpha\dagger} c_{j,\downarrow}^\alpha + \rho_\downarrow^\alpha c_{j,\uparrow}^{\alpha\dagger} c_{j,\uparrow}^\alpha \right\rangle_{\text{trial}} \\
 &+ \left\langle \sum_{j,\alpha} \Delta^\alpha c_{j,\downarrow}^{\alpha\dagger} c_{j,\uparrow}^{\alpha\dagger} + \Delta^{\alpha*} c_{j,\uparrow}^\alpha c_{j,\downarrow}^\alpha \right\rangle_{\text{trial}}, \tag{A2}
 \end{aligned}$$

where $\langle \dots \rangle_{\text{trial}}$ denotes expectation values with respect to the weight $e^{-\beta H_{\text{trial}}}/Z_{\text{trial}}$ with $Z_{\text{trial}} = \text{Tr} e^{-\beta H_{\text{trial}}} = e^{-\beta F_{\text{trial}}}$. Minimizing the right-hand side with respect to the MF variational parameters, we obtain an upper bound on the true free energy, which we define as the mean field free energy F_{MF} ,

$$F_{\text{MF}} = F_{\text{trial}} + UL \sum_{\alpha} \left(\rho_\uparrow^\alpha \rho_\downarrow^\alpha + \left| \frac{\Delta^\alpha}{U} \right|^2 \right), \tag{A3}$$

where $F_{\text{MF}} = \langle H_{\text{MF}} \rangle$ and $F_{\text{trial}} = \langle H_{\text{trial}} \rangle$ at $T = 0$. The mean field parameters can be expressed, following the optimization, as

$$\begin{aligned}
 \rho_\sigma^\alpha &= \langle c_{j,\sigma}^{\alpha\dagger} c_{j,\sigma}^\alpha \rangle, \\
 \Delta^\alpha &= U \langle c_{j,\uparrow}^\alpha c_{j,\downarrow}^\alpha \rangle. \tag{A4}
 \end{aligned}$$

This defines H_{MF} as

$$\begin{aligned}
 H_{\text{MF}} &= \sum_{i,j,\alpha,\sigma} (t_{ij}^{\alpha,\alpha'} c_{i,\sigma}^{\alpha\dagger} c_{j,\sigma}^{\alpha'} + \text{H.c.}) \\
 &- U \sum_{j,\alpha} \rho_\uparrow^\alpha c_{j,\downarrow}^{\alpha\dagger} c_{j,\downarrow}^\alpha + \rho_\downarrow^\alpha c_{j,\uparrow}^{\alpha\dagger} c_{j,\uparrow}^\alpha \\
 &- \sum_{j,\alpha} \Delta^\alpha c_{j,\downarrow}^{\alpha\dagger} c_{j,\uparrow}^{\alpha\dagger} + \Delta^{\alpha*} c_{j,\uparrow}^\alpha c_{j,\downarrow}^\alpha \\
 &- \mu \sum_{j,\alpha,\sigma} c_{j,\sigma}^{\alpha\dagger} c_{j,\sigma}^\alpha \\
 &+ L \sum_{\alpha} U \rho_\uparrow^\alpha \rho_\downarrow^\alpha + \frac{|\Delta^\alpha|^2}{U}. \tag{A5}
 \end{aligned}$$

With equal population of \uparrow - and \downarrow -spins, we can choose to replace $\rho_\uparrow^\alpha = \rho_\downarrow^\alpha = \rho^\alpha$. To study the superfluid behavior of the system, we apply a phase twist Φ with $c_{j,\sigma}^\alpha \rightarrow c_{j,\sigma}^\alpha e^{ij\Phi/L}$. In general, we can write the Fourier transformed mean-field Hamiltonian with a phase gradient as

$$\begin{aligned}
 H_{\text{MF}}(\Phi) &= \sum_k \Psi_k^\dagger \mathcal{M}_k(\Phi) \Psi_k \\
 &+ L \sum_{\alpha} \left(U \rho_\uparrow^\alpha \rho_\downarrow^\alpha + \frac{|\Delta^\alpha|^2}{U} - U \rho_\downarrow^\alpha - \mu \right), \tag{A6}
 \end{aligned}$$

with $\Psi_k^\dagger = (c_{k\uparrow}^{A\dagger} \ c_{k\uparrow}^{B\dagger} \ c_{k\uparrow}^{C\dagger} \ c_{-k\downarrow}^A \ c_{-k\downarrow}^B \ c_{-k\downarrow}^C)$ the Nambu spinor and the block matrix

$$\mathcal{M}_k(\Phi) = \begin{pmatrix} \mathcal{K}(\phi+k) & \mathcal{D} \\ \mathcal{D}^* & -\mathcal{K}^T(\phi-k) \end{pmatrix}. \tag{A7}$$

The block \mathcal{D} simply takes into account the pairing order parameter

$$\mathcal{D} = \begin{pmatrix} \Delta^A & 0 & 0 \\ 0 & \Delta^B & 0 \\ 0 & 0 & \Delta^C \end{pmatrix}. \quad (\text{A8})$$

The block $\mathcal{K}(\phi \pm k)$ expresses the hopping terms and sublattice-dependent filling as a modification to the chemical potential

$$\mathcal{K}(\phi + k) = \begin{pmatrix} K_{11} - \tilde{\mu}^A & K_{12} & K_{13} \\ K_{21} & K_{22} - \tilde{\mu}^B & K_{23} \\ K_{31} & K_{32} & K_{33} - \tilde{\mu}^C \end{pmatrix}, \quad (\text{A9})$$

where the sublattice-dependent chemical potential $\tilde{\mu}^\alpha = \mu + \rho^\alpha U$ is crucial to describe accurately a system with nonidentical sublattices. Here $K_{11} = 2t_a \cos(\phi + k)$, $K_{22} = 2t_e \cos(\phi + k)$, and $K_{33} = 2t_i \cos(\phi + k)$ are intercell hopping terms on the same sublattice. Further, $K_{12} = t_1 + t_b e^{i(\phi+k)} + t_d e^{-i(\phi+k)} = K_{21}^*$, $K_{23} = t_2 + t_f e^{i(\phi+k)} + t_h e^{-i(\phi+k)} = K_{32}^*$, and $K_{13} = t_3 + t_c e^{i(\phi+k)} + t_g e^{-i(\phi+k)} = K_{31}^*$.

APPENDIX B: CONSTRUCTION OF FLAT BAND HAMILTONIANS

We now outline the method to construct Hamiltonians with a flat band in the ground state [19] and show how to fix the

The winding number is given by

$$\begin{aligned} W\pi &= i \int_0^{2\pi} dk \langle \Psi_k | \partial_k \Psi_k \rangle \\ &= \frac{1}{2} \int_0^{2\pi} dk \left(1 + \frac{x^2 + y^2 + z^2 - a^2 - b^2 - c^2}{2 \cos(k) + a^2 + b^2 + c^2 + x^2 + y^2 + z^2} \right) \\ &= \pi + \frac{\pi(x^2 + y^2 + z^2 - a^2 - b^2 - c^2)}{\sqrt{(a^2 + b^2 + c^2 + x^2 + y^2 + z^2)^2 - 4}}. \end{aligned} \quad (\text{B6})$$

We see that by choosing Ψ_1 and Ψ_2 appropriately, one can tune to the desired value of W . The integral over the Brillouin zone of the quantum metric can now be expressed as

$$Q = \frac{1}{2\pi} \int_0^{2\pi} \text{Re}[g(k)] dk = \frac{(a^2 + b^2 + c^2 + x^2 + y^2 + z^2)[(a^2 + b^2 + c^2)^2 + (x^2 + y^2 + z^2)^2 - 2]}{[(a^2 + b^2 + c^2 + x^2 + y^2 + z^2)^2 - 4]^{3/2}}, \quad (\text{B7})$$

with $g(k) = 2(\langle \partial_k \Psi_k | \partial_k \Psi_k \rangle - |\langle \Psi_k | \partial_k \Psi_k \rangle|^2)$ the quantum geometric tensor and its real part the quantum metric. To find the hopping potentials, we choose a flat band energy E_{FB} and satisfy the conditions in Ref. [19].

For a real CLS, the two equations to solve for intracell hopping terms are

$$\begin{aligned} E_{\text{FB}} &= \langle \Psi_2 | H_0 | \Psi_1 \rangle \\ &= t_1(bx + ay) + t_2(cy + bz) + t_3(cx + az) \end{aligned} \quad (\text{B8})$$

and

$$\langle \Psi_1 | E_{\text{FB}} - H_0 | \Psi_1 \rangle = \langle \Psi_2 | E_{\text{FB}} - H_0 | \Psi_2 \rangle. \quad (\text{B9})$$

The expression for H_1 is

$$H_1 = \frac{(E_{\text{FB}} - H_0) | \Psi_1 \rangle \langle \Psi_2 | (E_{\text{FB}} - H_0)}{\langle \Psi_1 | E_{\text{FB}} - H_0 | \Psi_1 \rangle} + Q_{12} K Q_{12}. \quad (\text{B10})$$

winding number. The most general form of the CLS on two unit cells is

$$\Psi_1 = \begin{pmatrix} a \\ be^{i\beta} \\ ce^{i\gamma} \end{pmatrix}, \quad \Psi_2 = \begin{pmatrix} xe^{i\chi} \\ ye^{i\tau} \\ ze^{i\zeta} \end{pmatrix}. \quad (\text{B1})$$

The first condition is to have [19]

$$\langle \Psi_1 | \Psi_2 \rangle = axe^{i(\chi)} + b ye^{i(\tau-\beta)} + c ze^{i(\zeta-\gamma)} = 1. \quad (\text{B2})$$

We obtain the Bloch state by Fourier transforming, which can be written as

$$|\Psi_k\rangle = \frac{1}{R} \begin{pmatrix} a + xe^{i(\chi-k)} \\ be^{i\beta} + ye^{i(\tau-k)} \\ ce^{i\gamma} + ze^{i(\zeta-k)} \end{pmatrix}. \quad (\text{B3})$$

To normalize the Bloch state, the expression which gives R is

$$R^2 = 2 \cos(k) + a^2 + b^2 + c^2 + x^2 + y^2 + z^2. \quad (\text{B4})$$

Differentiating the normalized Bloch state with respect to the lattice momentum, we obtain

$$|\partial_k \Psi_k\rangle = \frac{1}{R^3} \begin{pmatrix} (a + xe^{i(\chi-k)}) \sin(k) - iR^2 xe^{i(\chi-k)} \\ (be^{i\beta} + ye^{i(\tau-k)}) \sin(k) - iR^2 ye^{i(\tau-k)} \\ (ce^{i\gamma} + ze^{i(\zeta-k)}) \sin(k) - iR^2 ze^{i(\zeta-k)} \end{pmatrix}. \quad (\text{B5})$$

The term K is arbitrary and Q_{12} is constructed from the CLS,

$$\begin{aligned} Q_{12} &= R_{12} Q_1, \\ Q_i &= \mathbb{I} - \frac{|\Psi_i\rangle \langle \Psi_i|}{\langle \Psi_i | \Psi_i \rangle}, \\ R_{12} &= \mathbb{I} - \frac{Q_1 | \Psi_2 \rangle \langle \Psi_2 | Q_1}{\langle \Psi_2 | Q_1 | \Psi_2 \rangle}. \end{aligned} \quad (\text{B11})$$

In general, for a chosen winding number, there is thus an infinite number of flat band lattices that can be constructed.

Equation (B6) shows how to tune the winding number to a desired value. To obtain $W = 0$, we obtain the condition

$$|\Psi_1|^2 |\Psi_2|^2 = (a^2 + b^2 + c^2)(x^2 + y^2 + z^2) = 1. \quad (\text{B12})$$

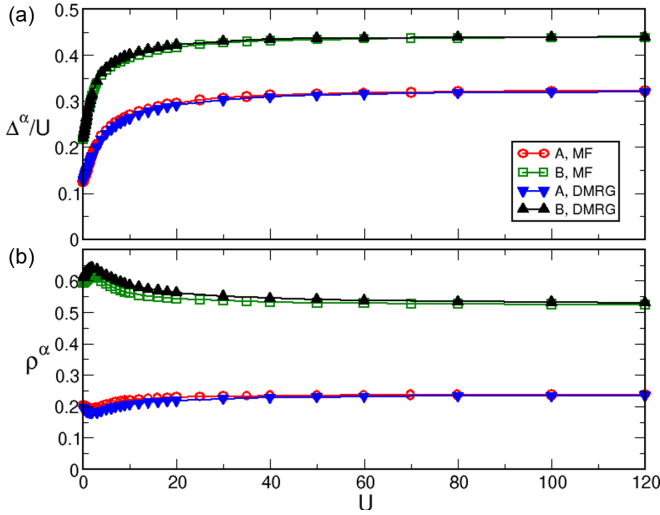


FIG. 11. Order parameter and sublattice fillings for the isolated flat band of lattice \mathcal{A} ($\kappa = 0$) with $\rho = \frac{1}{3}$. (a) Order parameters acquire a large nonzero value for any finite U , and $\Delta^A/U = \Delta^C/U$ for $\Phi = 0$. (b) Sublattice fillings ρ^α are shown to be sublattice dependent, and this can only be properly reproduced with the MF method when ρ^α are considered as MF parameters.

This gives the normalization condition

$$\langle \Psi_1 | \Psi_2 \rangle = 1 = |\Psi_1 | \Psi_2 | \cos(\theta) = \cos(\theta), \quad (\text{B13})$$

which implies that $|\Psi_1\rangle = M|\Psi_2\rangle$, where M is a constant; M can simply be expressed through

$$|\Psi_1\rangle = |\Psi_2\rangle \langle \Psi_1 | \Psi_1 \rangle. \quad (\text{B14})$$

From Eq. (B10) we consider the denominator $\langle \Psi_1 | E_{\text{FB}} - H_0 | \Psi_1 \rangle$,

$$\begin{aligned} \langle \Psi_1 | E_{\text{FB}} - H_0 | \Psi_1 \rangle &= E_{\text{FB}} \langle \Psi_1 | \Psi_1 \rangle - \langle \Psi_1 | H_0 | \Psi_1 \rangle \\ &= E_{\text{FB}} \langle \Psi_1 | \Psi_1 \rangle - \langle \Psi_1 | H_0 | \Psi_2 \rangle \langle \Psi_1 | \Psi_1 \rangle \end{aligned}$$

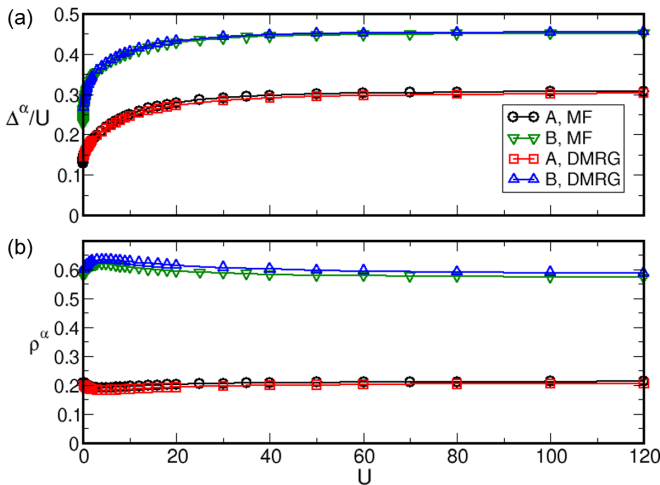


FIG. 12. Order parameter and sublattice fillings for the nonisolated flat band of lattice \mathcal{A} ($\kappa = -0.375$) with $\rho = \frac{1}{3}$. (a) Order parameters are sublattice dependent with $\Delta^A/U = \Delta^C/U$ for $\Phi = 0$. (b) Sublattice fillings ρ^α .

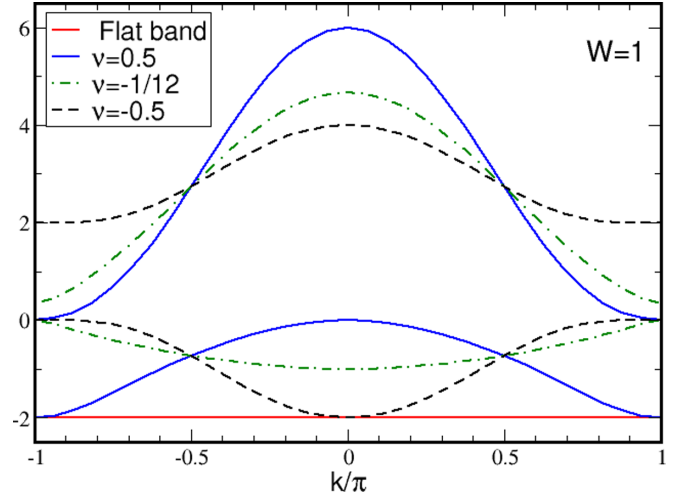


FIG. 13. Band structure of lattice \mathcal{B} .

$$\begin{aligned} &= E_{\text{FB}} \langle \Psi_1 | \Psi_1 \rangle - E_{\text{FB}} \langle \Psi_1 | \Psi_1 \rangle \\ &= 0. \end{aligned} \quad (\text{B15})$$

This means that for a finite H_1 , we have an additional condition that $(E_{\text{FB}} - H_0)|\Psi_1\rangle \langle \Psi_2 | (E_{\text{FB}} - H_0) = 0$. To determine $H_1 = Q_{12}KQ_{12}$, we can work out that $Q_1|\Psi_2\rangle = 0$ and $R_{12} = \mathbb{I}$. To show that the CLS is localized within one unit cell,

$$H_1|\Psi_1\rangle = Q_1KQ_1|\Psi_1\rangle = 0. \quad (\text{B16})$$

For a lattice with $W = 0$ and a chosen real CLS and E_{FB} , there is a unique solution for the intracell hopping terms, and we can only have the CLS localized within one unit cell.

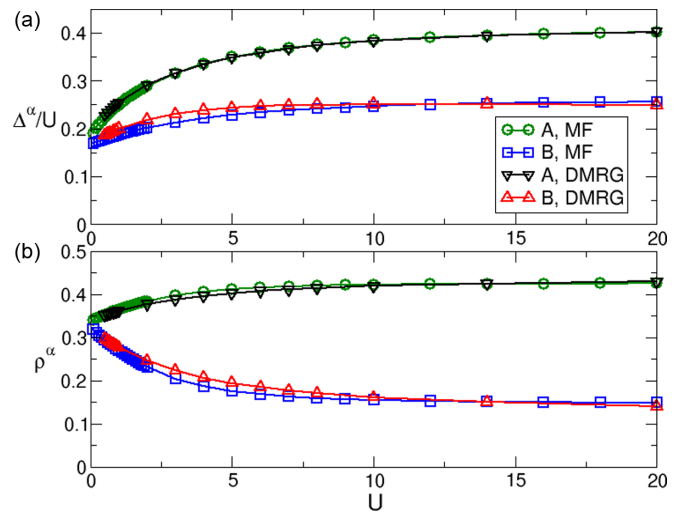


FIG. 14. (a) Pairing order parameter and (b) sublattice fillings for lattice \mathcal{C} ($W = 0$), touching bands with $q = 1.5$. While the values of D_s calculated using the MF and DMRG methods agree well qualitatively and less well quantitatively, the order parameter and sublattice fillings are accounted for very well by the full mean field method. The filling is $\rho = \frac{1}{3}$.

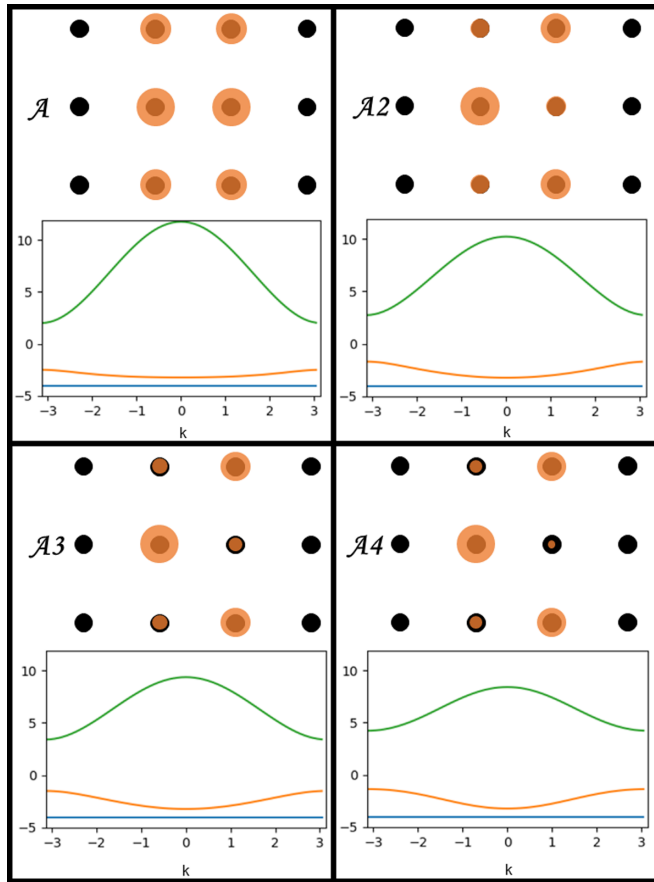


FIG. 15. The CLS is increasingly asymmetrical from lattice \mathcal{A} to $\mathcal{A}4$. The flat band energy is kept constant at -4 , the band gap is $E_{\text{gap}} \approx 0.7625$, and $W = 1$.

APPENDIX C: BAND STRUCTURE AND ORDER PARAMETERS

1. Lattice \mathcal{A}

Figures 11 and 12 show the agreement between the DMRG and full MF calculations for the order parameters and sublattice fillings for both the gapped and gapless cases of lattice \mathcal{A} ($W = 1$) studied in Sec. III. Note that the order parameters Δ^α/U acquire a large finite value once U is nonzero, while $\Delta^\alpha \propto U$ linearly. An important point to note is the sublattice fillings, where sublattices A and C have equal filling but sublattice B is different. This is only faithfully reproduced in the MF method that we propose and not when the BCS MF method is employed (Appendix E).

2. Lattice \mathcal{B}

The band structures of lattice \mathcal{B} ($W = 1$) for cases where we computed D_s (Fig. 5) are shown in Fig. 13. The bands touch at $k = 0$ for $\nu = -0.5$ and $k = \pi$ for $\nu = 0.5$; the gapped case with $E_{\text{gap}} = 1$ has $\nu = -\frac{1}{12}$.

3. Lattice \mathcal{C}

In Fig. 14 we show, for lattice \mathcal{C} touching bands with $\rho = 1.5$, that although the D_s computed with the MF and DMRG

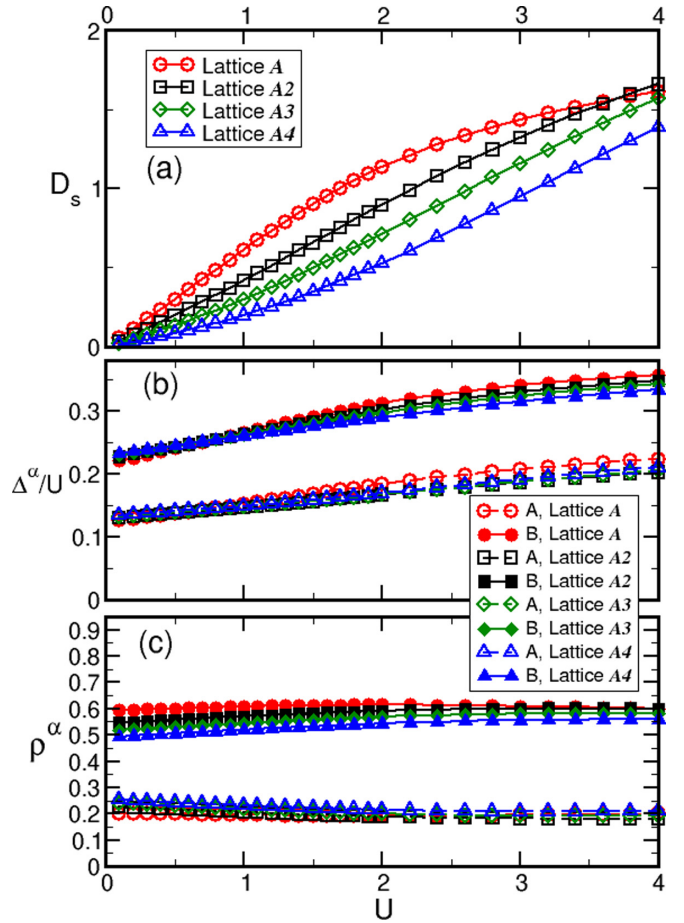


FIG. 16. Parameters D_s , ρ^α , and Δ^α for lattices \mathcal{A} , $\mathcal{A}2$, $\mathcal{A}3$, and $\mathcal{A}4$ (Fig. 15) obtained through MF computation. The pairing order parameters, site fillings, and integral over the BZ of the quantum metric vary slightly, while the superfluid density is evidently distinct for the cases considered. The filling is $\rho = \frac{1}{3}$.

methods agree well qualitatively but less so quantitatively for the nontopological flat bands ($W = 0$), the pairing order parameter and sublattice fillings are modeled very well by the full mean field method. The agreement between MF and DMRG calculations for Δ^α and ρ^α was also observed for the isolated nontopological flat band.

APPENDIX D: OTHER LATTICES

Here we show that D_s is strongly dependent on the CLS. We consider lattice \mathcal{A} ($W = 1$) and tune the CLS while keeping $E_{\text{FB}} = -4$, $E_{\text{gap}} \approx 0.7625$, $t_2 = \sqrt{7}$, and $t_3 = 1$ constant, through the change of H_1 and t_1 . The CLS and band structures that we consider are shown in Fig. 15, labeled lattices \mathcal{A} , $\mathcal{A}2$, $\mathcal{A}3$, and $\mathcal{A}4$, with increasing asymmetry of the CLS.

We compute D_s , sublattice fillings and order parameters with the MF method for these lattices and show that while ρ^α and Δ^α do not vary significantly [Figs. 16(b) and 16(c)], D_s changes substantially across the cases considered [Fig. 16(a)]. In general, the slope is largest for the most symmetric CLS, which also has the fastest exponential decay of the Wannier function (not shown). Moreover, symmetric occupation of CLS leads to larger overlap of the Wannier functions. This can

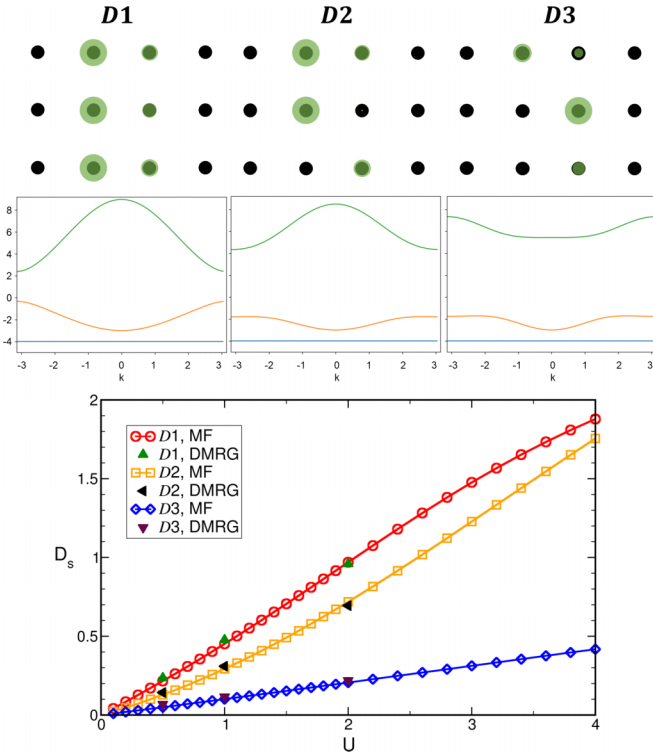


FIG. 17. Plot of D_s vs U for $W = 0.5$ and $\rho = \frac{1}{3}$, with corresponding band structures and CLS depicting various asymmetries. We include DMRG points showing the agreement of the full MF calculation at finite noninteger winding.

serve as a guide to optimizing superconductivity by engineering the Hamiltonian which corresponds to the most symmetric localized state. We emphasize that while the winding number is constant and the integral over the BZ of the quantum metric does not vary much ($\mathcal{Q}_{A1} = 0.505$, $\mathcal{Q}_{A2} = 0.507$, $\mathcal{Q}_{A3} = 0.509$, and $\mathcal{Q}_{A4} = 0.516$), the slopes of D_s [Fig. 16(a)] are evidently distinct. Additionally, for lattice \mathcal{B} with symmetric CLS and equal filling on all CLS sites, the slope at low U is equal to that of lattice \mathcal{A} .

The MF and DMRG agreement extends to lattices with noninteger finite winding. Again, with equal $E_{\text{gap}} = 1$, $E_{\text{FB}} = -4$, and similar band structures, we show that D_s is dependent on the CLS (Fig. 17). For a winding of $W = 0.5$, we obtain an asymmetric CLS and give three examples: lattices $\mathcal{D}1$, $\mathcal{D}2$, and $\mathcal{D}3$. Note that for $W = 0.5$, the CLS cannot be symmetric but the degree of the asymmetry can be tuned. To eliminate the effects contributed through the uppermost band, we focus on the range $0 < U \leq 4$. We propose that the optimization of D_s is contingent on occupation of the CLS, where one should identify the model with filling most symmetric on all sublattices. This means that if some sublattice occupations of the CLS are zero, D_s will be significantly reduced.

APPENDIX E: FAILING OF THE MF WITHOUT ρ^α AS A MF PARAMETER

We have insisted repeatedly on the importance of including the site-dependent fillings as MF parameters. Here we show how the BCS approach fails when taken with the correct

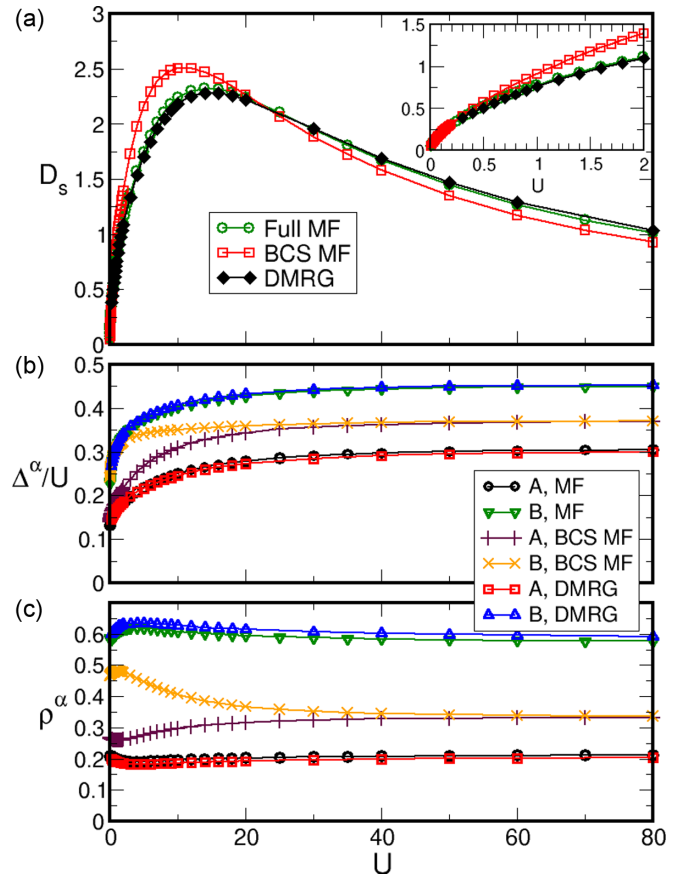


FIG. 18. Lattice \mathcal{A} ($W = 1$) gapless at $k = 0$ ($\kappa = -0.375$). The BCS MF approach without sublattice densities as mean field parameters compared with the full MF and DMRG calculations shows a clear disagreement. (a) The plot of D_s as a function of U obtained from the BCS MF calculation agrees for very weak interactions (inset) but quickly deviates from the full MF and DMRG results. The discrepancy is especially prominent in (b), which shows the order parameter, and (c), which shows the site fillings, where the BCS MF method inaccurately models sublattices with equivalent Δ^α and ρ^α at large U . The filling is $\rho = \frac{1}{3}$.

complex order parameters but without the site densities. In the BCS MF approach, which has been extensively employed in many studies [10,15–17], the Hubbard interaction term is simply decomposed as

$$-U c_{j,\downarrow}^{\alpha\dagger} c_{j,\uparrow}^{\alpha\dagger} c_{j,\uparrow}^{\alpha} c_{j,\downarrow}^{\alpha} = -\Delta^\alpha c_{j,\downarrow}^{\alpha\dagger} c_{j,\uparrow}^{\alpha\dagger} + \Delta^{\alpha*} c_{j,\uparrow}^{\alpha} c_{j,\downarrow}^{\alpha} + \frac{|\Delta^\alpha|^2}{U}. \quad (\text{E1})$$

In general, for the BCS MF calculations, the site densities will go to the same value $\rho^\alpha \rightarrow \rho$ as U increases. As a result, the order parameters Δ^α for the sublattices will also tend to the same value at large U . This is both qualitatively and quantitatively wrong, as we have presented in Appendix C, where sublattices continue to be inequivalent even at large U .

As an example, we show in Fig. 18 a comparison of full multiband MF, BCS MF, and DMRG results for the gapless case ($\kappa = -0.375$) of lattice \mathcal{A} ($W = 1$). At weak coupling, we find that the BCS MF does not capture the actual behavior of D_s well, with the inaccurate power dependence evident in

the inset. As U increases, the disagreement becomes increasingly apparent.

Consequently, while one can focus on the superfluid weight (and its relation to the quantum metric) calculated

through the BCS MF method and argue that it is in acceptable agreement, a closer look at the sublattice equivalence and properties reveals the breakdown of this approach.

-
- [1] Y. Cao, V. Fatemi, S. Fang, K. Watanabe, T. Taniguchi, E. Kaxiras, and P. Jarillo-Herrero, *Nature (London)* **556**, 43 (2018).
- [2] Y. Cao, V. Fatemi, A. Demir, S. Fang, S. L. Tomarken, J. V. Luo, J. D. Sanchez-Yamagishi, K. Watanabe, T. Taniguchi, E. Kaxiras, R. C. Ashoori, and P. Jarillo-Herrero, *Nature (London)* **556**, 80 (2018).
- [3] M. Yankowitz, S. Chen, H. Polshyn, Y. Zhang, K. Watanabe, T. Taniguchi, D. Graf, A. F. Young, and C. R. Dean, *Science* **363**, 1059 (2019).
- [4] J. M. Park, Y. Cao, K. Watanabe, T. Taniguchi, and P. Jarillo-Herrero, *Nature (London)* **590**, 249 (2021).
- [5] V. Khodel and V. Shaginyan, *JETP Lett.* **51**, 553 (1990).
- [6] S. Peotta and P. Törmä, *Nat. Commun.* **6**, 8944 (2015).
- [7] N. B. Kopnin, T. T. Heikkilä, and G. E. Volovik, *Phys. Rev. B* **83**, 220503(R) (2011).
- [8] R. Mondaini, G. G. Batrouni, and B. Grémaud, *Phys. Rev. B* **98**, 155142 (2018).
- [9] S. M. Chan, B. Grémaud, and G. G. Batrouni, *Phys. Rev. B* **105**, 024502 (2022).
- [10] K.-E. Huhtinen, J. Herzog-Arbeitman, A. Chew, B. A. Bernevig, and P. Törmä, *Phys. Rev. B* **106**, 014518 (2022).
- [11] M. Tovmasyan, S. Peotta, L. Liang, P. Törmä, and S. D. Huber, *Phys. Rev. B* **98**, 134513 (2018).
- [12] V. A. J. Pyykkönen, S. Peotta, P. Fabritius, J. Mohan, T. Esslinger, and P. Törmä, *Phys. Rev. B* **103**, 144519 (2021).
- [13] T. T. Heikkilä, N. B. Kopnin, and G. E. Volovik, *JETP Lett.* **94**, 233 (2011).
- [14] S. Miyahara, S. Kusuta, and N. Furukawa, *Physica C* **460–462**, 1145 (2007).
- [15] M. Iskin, *Phys. Rev. A* **99**, 053608 (2019).
- [16] Y.-R. Wu, X.-F. Zhang, C.-F. Liu, W.-M. Liu, and Y.-C. Zhang, *Sci. Rep.* **11**, 1 (2021).
- [17] A. Julku, S. Peotta, T. I. Vanhala, D.-H. Kim, and P. Törmä, *Phys. Rev. Lett.* **117**, 045303 (2016).
- [18] N. Verma, T. Hazra, and M. Randeria, *Proc. Natl. Acad. Sci. USA* **118**, e2106744118 (2021).
- [19] W. Maimaiti, S. Flach, and A. Andreanov, *Phys. Rev. B* **99**, 125129 (2019).
- [20] S. Xia, Y. Hu, D. Song, Y. Zong, L. Tang, and Z. Chen, *Opt. Lett.* **41**, 1435 (2016).
- [21] Y. Zong, S. Xia, L. Tang, D. Song, Y. Hu, Y. Pei, J. Su, Y. Li, and Z. Chen, *Opt. Express* **24**, 8877 (2016).
- [22] S. Mukherjee, A. Spracklen, D. Choudhury, N. Goldman, P. Öhberg, E. Andersson, and R. R. Thomson, *Phys. Rev. Lett.* **114**, 245504 (2015).
- [23] S. Mukherjee and R. R. Thomson, *Opt. Lett.* **42**, 2243 (2017).
- [24] F. Baboux, L. Ge, T. Jacqmin, M. Biondi, F. Galopin, A. Lemaître, L. Le Gratiet, I. Sagnes, S. Schmidt, H. E. Türeci, A. Amo, and J. Bloch, *Phys. Rev. Lett.* **116**, 066402 (2016).
- [25] M. E. Fisher, M. N. Barber, and D. Jasnow, *Phys. Rev. A* **8**, 1111 (1973).
- [26] X. Zotos, P. Prelovsek, and I. Sega, *Phys. Rev. B* **42**, 8445 (1990).
- [27] B. S. Shastry and B. Sutherland, *Phys. Rev. Lett.* **65**, 243 (1990).
- [28] D. J. Scalapino, S. R. White, and S. Zhang, *Phys. Rev. B* **47**, 7995 (1993).
- [29] C. A. Hayward, D. Poilblanc, R. M. Noack, D. J. Scalapino, and W. Hanke, *Phys. Rev. Lett.* **75**, 926 (1995).
- [30] B. Grémaud and G. G. Batrouni, *Phys. Rev. Lett.* **127**, 025301 (2021).
- [31] A. F. Albuquerque, F. Alet, P. Corboz, P. Dayal, A. Feiguin, S. Fuchs, L. Gamper, E. Gull, S. Gürtler, A. Honecker *et al.*, *J. Magn. Magn. Mater.* **310**, 1187 (2007).
- [32] B. Bauer, L. D. Carr, H. G. Evertz, A. Feiguin, J. Freire, S. Fuchs, L. Gamper, J. Gukelberger, E. Gull, S. Guertler, and A. Hehn, *J. Stat. Mech.* (2011) P05001.
- [33] V. Emery, *Phys. Rev. B* **14**, 2989 (1976).
- [34] C. Triola, J. Cayao, and A. M. Black-Schaffer, *Ann. Phys. (Berlin)* **532**, 1900298 (2020).
- [35] A. L. Kuzemsky, *Int. J. Mod. Phys. B* **29**, 1530010 (2015).